

# NAVAL POSTGRADUATE SCHOOL

## Monterey, California

AD-A205 936



# THESIS

**STRESS RELIEF CRACKING IN  
COPPER-PRECIPITATION STRENGTHENED  
HSLA-100 STEEL**

by

Steven A. McNutt

December 1988

Thesis Co-Advisors:

Saeed Saboury  
J. M. B. Losz

Approved for public release; distribution is unlimited.

DTIC  
ELECTE  
MAR 28 1989  
S H D

Unclassified

Security Classification of this page

REPORT DOCUMENTATION PAGE				
1a Report Security Classification <b>Unclassified</b>		1b Restrictive Markings		
2a Security Classification Authority		3 Distribution Availability of Report <b>Approved for public release; distribution is unlimited.</b>		
2b Declassification/Downgrading Schedule		5 Monitoring Organization Report Number(s)		
4 Performing Organization Report Number(s)		7a Name of Monitoring Organization Naval Postgraduate School		
6a Name of Performing Organization Naval Postgraduate School	6b Office Symbol (If Applicable) 69	7b Address (city, state, and ZIP code) Monterey, CA 93943-5000		
6c Address (city, state, and ZIP code) Monterey, CA 93943-5000		9 Procurement Instrument Identification Number		
8a Name of Funding/Sponsoring Organization	8b Office Symbol (If Applicable)	10 Source of Funding Numbers		
8c Address (city, state, and ZIP code)		Program Element Number	Project No	Task No
		Work Unit Accession No		
11 Title (Include Security Classification) <b>Stress Relief Cracking in Copper-Precipitation Strengthened HSLA-100 Steel</b>				
12 Personal Author(s) <b>Steven McNutt</b>				
13a Type of Report Master's Thesis	13b Time Covered From To	14 Date of Report (year, month, day) December 1988	15 Page Count: 99	
16 Supplementary Notation The views expressed in this thesis are those of the author and do not reflect the official policy or position of the Department of Defense or the U.S. Government.				
17 Cosati Codes		18 Subject Terms (continue on reverse if necessary and identify by block number)		
Field	Group	Subgroup	Stress Relief Cracking; HSLA-100 Steel, Copper-Precipitation Strengthened Steel	
19 Abstract (continue on reverse if necessary and identify by block number) The US Navy is currently developing a new family of high-strength, low-alloy steels which derive a significant portion of their strength from copper precipitation. These highly weldable steels require little or no preheat, resulting in substantial cost savings. The first of these steels, HSLA-80, has been certified for ship construction, but recent studies have indicated some susceptibility to stress relief cracking in weldments. HSLA-100, a modification of HSLA-80, is now being considered for several higher-strength naval structures. Stress-relief cracking has not been studied previously in this steel and is the subject of investigation in this work. The steel weldments were loaded below their yield strength, heated to temperatures of 550°-650° C, and permitted to stress relieve for one hour. At all temperatures, the steel exhibited susceptibility to stress relief cracking in certain stress ranges. Optical and scanning electron microscopy exhibited intergranular cracking which always traversed the coarse-grained region of the heat-affected zone. Auger and transmission electron microscopy indicated high concentrations of alloying elements at the grain boundaries. Stress-relief cracking was associated with the diffusion of alloying elements to the prior austenite grain boundaries.				
20 Distribution/Availability of Abstract <input checked="" type="checkbox"/> unclassified/unlimited <input type="checkbox"/> same as report <input type="checkbox"/> DTIC users		21 Abstract Security Classification <b>Unclassified</b>		
22a Name of Responsible Individual Professor S. Saboury		22b Telephone (Include Area code) (408) 646-2656	22c Office Symbol 69Ss	

DD FORM 1473, 83 MAR

83 APR edition may be used until exhausted

security classification of this page

All other editions are obsolete

Unclassified

Approved for public release; distribution is unlimited.

**Stress Relief Cracking in Copper-Precipitation  
Strengthened HSLA-100 Steel**

by

Steven A. McNutt  
Captain, Canadian Forces  
B.E.Sc. (Materials), University of Western Ontario, 1980


Submitted in partial fulfillment of the  
requirements for the degree of

MASTER OF SCIENCE IN MECHANICAL ENGINEERING

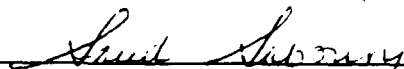
from the

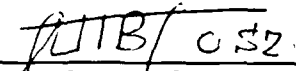
NAVAL POSTGRADUATE SCHOOL  
December 1988

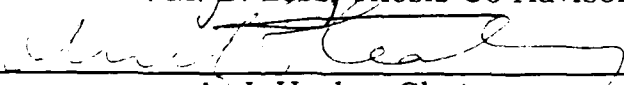
Author:

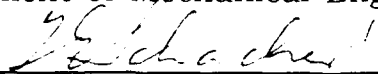
  
Steven A. McNutt

Approved by:

  
Saeed Saboury, Thesis Co-Advisor

  
J. M. B. Losz, Thesis Co-Advisor

  
A. J. Healey, Chairman,  
Department of Mechanical Engineering

  
Gordon E. Schacher, Dean of  
Science and Engineering

## ABSTRACT

The US Navy is currently developing a new family of high-strength, low-alloy steels which derive a significant portion of their strength from copper precipitation. These highly weldable steels require little or no preheat, resulting in substantial cost savings. The first of these steels, HSLA-80, has been certified for ship construction, but recent studies have indicated some susceptibility to stress relief cracking in weldments.

HSLA-100, a modification of HSLA-80, is now being considered for several higher-strength naval structures. Stress-relief cracking has not been studied previously in this steel and is the subject of investigation in this work. The steel weldments were loaded below their yield strength, heated to temperatures of 550°-650° C, and permitted to stress relieve for one hour. At all temperatures, the steel exhibited susceptibility to stress relief cracking in certain stress ranges. Optical and scanning electron microscopy exhibited intergranular cracking which always traversed the coarse-grained region of the heat-affected zone. Auger and transmission electron microscopy indicated high concentrations of alloying elements at the grain boundaries. Stress-relief cracking was associated with the diffusion of alloying elements to the prior austenite grain boundaries.



Accession For	
NTIS GPA&I	<input checked="" type="checkbox"/>
ETIC TAB	<input type="checkbox"/>
Unannounced	<input type="checkbox"/>
Justification	
By	
Distribution/	
Availability Codes	
Avail and/or	
Dist	Special
A-1	

## TABLE OF CONTENTS

<b>I. INTRODUCTION.....</b>	<b>1</b>
<b>II. BACKGROUND .....</b>	<b>3</b>
A. NAVAL PERSPECTIVE.....	3
B. HSLA-100 ALLOY DESIGN.....	5
C. ROLE OF COPPER.....	8
D. STRESS-RELIEF CRACKING.....	12
E. WELDING OF HSLA-100 STEEL.....	17
F. FILLER METAL/ELECTRODE.....	18
G. APPLICATIONS.....	20
<b>III. EXPERIMENTAL PROCEDURE.....</b>	<b>21</b>
A. MATERIAL.....	21
B. SAMPLE PREPARATION.....	21
C. MICROHARDNESS MEASUREMENTS.....	25
D. OPTICAL MICROSCOPY.....	25
E. SCANNING ELECTRON FRACTOGRAPHY.....	26
F. AUGER ELECTRON SPECTROSCOPY.....	26
G. TRANSMISSION ELECTRON MICROSCOPY.....	26
H. TEST APPARATUS.....	27

I.	TEMPERATURE MEASUREMENT AND CONTROL.....	29
J.	TESTING PROCEDURE.....	32
<b>IV.</b>	<b>EXPERIMENTAL RESULTS.....</b>	<b>37</b>
A.	MACROSTRUCTURE.....	37
B.	MICROHARDNESS MEASUREMENTS.....	37
C.	MICROSTRUCTURE IN THE AS-RECEIVED WELDMENT.....	42
1.	Weld Metal.....	42
2.	Coarse-Grained Heat-Affected Zone.....	42
3.	Fusion Line.....	48
4.	Fine-Grained Heat-Affected Zone.....	49
5.	Base Metal.....	49
D.	MICROSTRUCTURE AFTER STRESS-RELIEF TESTING.....	49
1.	Weld Metal.....	49
2.	Coarse-Grained Heat-Affected Zone.....	55
3.	Fusion Line.....	55
E.	ROOM-TEMPERATURE TENSILE TESTING.....	60
F.	STRESS-RELIEF CRACKING.....	60
G.	AUGER ELECTRON SPECTROSCOPY.....	70
<b>V.</b>	<b>DISCUSSION.....</b>	<b>76</b>
A.	MICROSTRUCTURE.....	76
B.	MICROHARDNESS PROFILES.....	78
C.	STRESS-RELIEF CRACKING.....	80

<b>VI. CONCLUSIONS.....</b>	<b>84</b>
LIST OF REFERENCES.....	85
INITIAL DISTRIBUTION LIST.....	89

## ACKNOWLEDGMENTS

I wish to express my appreciation to my thesis advisors, Dr. Saeed Saboury and Dr. J. Mauro Losz. A special thank you is extended to Saeed for his immeasurable guidance, dedication, sense of humor, and especially for his friendship. I would also like to acknowledge Mauro for his fine transmission electron microscopy work and Ken Ellison for his technical assistance.

A most sincere thank you is extended to Claudine Guerin and Robert Perron, who continually sacrificed their time to care for my daughters with love and understanding. I also thank my parents for their assistance after the birth of our two American daughters, enabling Teresa and me to complete our studies.

I would also like to express my appreciation for the excellent opportunity my branch and the Canadian Forces have given Teresa and me to continue our education.

Finally, I would like to thank my fellow student and wife for her support, tutoring, and love. I dedicate this thesis to you along with Kaitlyn and Megan, who have all sacrificed so much.



## I. INTRODUCTION

The US Navy has set as a goal the development and certification of a new family of high-strength, low-alloy (HSLA) steels by 1990. These copper-precipitation strengthened steels contain a low carbon content which makes them capable of being welded with little or no preheat. A quenched and aged condition enables the copper content to precipitate and further strengthen the steel. The replacement of the HY series of steels with these HSLA steels will result in enhancing the overall quality while significantly reducing the ship-building costs through the improvement of welding processes and materials technology.

The first of these steels, HSLA-80, is a derivative of ASTM A710 Grade A Class 3 steel. This steel is capable of providing yield strengths in the 552-621 MPa (80-90 Ksi) range and has been used on all substructures and on the hull of the cruisers Ticonderoga. Field experience in welding over 1,800 metric tons of this steel (1985 figure) and extensive welding and weldability research have not reported any form of cracking in the weldments [Refs. 1, 2, 3]. However, recent work on the Heat Affected Zone (HAZ) of ASTM A710 steel has indicated some susceptibility to cracking associated with post-weld stress relief treatment. Although the metallurgical causes for this failure have not been investigated in detail, the available results suggest that the

mechanisms of copper precipitation on the grain boundaries in the HAZ during thermal cycling may be involved. [Ref. 4]

Stress relief cracking has not been previously studied in HSLA-100 steel. In this investigation, the susceptibility of cracking in HSLA-100 weldments to post-weld heat treatment was studied. The composition of HSLA-100 is based upon that of HSLA-80, with some modification, and is designed for a 25 percent increase in strength. The thermal relief experiment was conducted through unidirectional loading of flat tensile specimens containing actual weldments in their gauge length. An induction coil was used for heating and a Materials Testing System (MTS) was utilized to apply and maintain the stress or strain. All testing was conducted at documented stress-relieving temperatures in an attempt to simulate real-life post-weld heat treatment conditions [Ref. 5]. Cracking was observed at all temperatures in relatively small stress ranges. The microstructural characteristics of the HAZ before and after testing were examined and compared using optical and electron microscopy. The results were then correlated with the measured mechanical properties.

## **II. BACKGROUND**

### **A. NAVAL PERSPECTIVE**

The overall weight must be optimized for a ship to perform at its maximum efficiency. A reduction in structural weight by the replacement of a lower-strength steel with a thinner, higher-strength material is a means of achieving this critical design consideration. This has been the major impetus of NAVSEA's material fabrication improvement goals for fiscal years 1983 through 1990. The aim of this program is to reduce ship-building costs through the improvement of: (1) welding processes, (2) materials processing technologies, and (3) fabrication techniques, while simultaneously improving overall quality. [Refs. 1, 2]

Most of the high-strength steels currently utilized by the US Navy (HY80, HY100) were developed over two decades ago when technology for producing extra low-carbon high-strength steels was not evolved to the extent it is today [Ref. 6]. These HY steels attain their strength levels from a tempered martensitic structure after a quench and temper heat treatment. The welding of these steels requires the use of preheat and controlled interpass temperatures to avoid hydrogen assisted cracking in the weldment. Adherence to these temperatures will also ensure the desired mechanical properties are obtained. These requirements increase the welding costs considerably. [Ref. 1]

High-strength ferritic steels have been successfully used for construction of pipelines and offshore platforms for several years. One of these steels, HSLA-80 (MIL-S-24645), a derivative of ASTM A710 Grade A Class 3, has recently been developed and certified for use on the cruisers of the Ticonderoga class, now under construction [Ref. 2]. Production experience has shown that HSLA-80 can be fabricated for a ship structure meeting military specifications while incurring substantial cost and weight savings [Refs. 1, 2]. Excellent weldability and toughness allow the welding of plates up to 19 mm (3/4") thick with no preheat [Ref. 7].

Based on the experience with HSLA-80, capable of 552-621 MPa (80-90 Ksi) yield strengths, the Navy started a research program to develop and certify a new higher-strength steel, HSLA-100. This new steel, capable of a 690 MPa (100 Ksi) yield strength, was to be a modification of HSLA-80. [Ref. 7]

The development of HSLA-100 was carried out by the AMAX Materials Research Center (AMRC) under contract N00167-85-C-0066 to the David Taylor Naval Ship Research and Development Center (DTNSRDC). The three phases of this program were:

- Phase I: Laboratory alloy development, interim specifications;
- Phase II: Trial production in quantity;
- Phase III: Plate production in quantity.

The laboratory phase of HSLA-100 development has been completed and interim specifications covering composition (Table 1), processing, and property requirements were prepared by AMRC. The

results of Phase I met the imposed stipulations that the new steel should be a quenched and aged, low-carbon, copper-precipitation strengthened steel with a 690 MPa minimum yield strength. This prerequisite was the basis for the trial commercial production of the 6 to 51 mm (0.25" to 2.0") thick plates by Phoenix Steel Corporation. Throughout this process, an effort was made to refine the composition to improve the methods of production and fabrication while retaining the mechanical properties. [Refs. 7, 8, 9]

TABLE 1  
INTERIM CHEMICAL COMPOSITIONS OF  
HSLA-100 IN WEIGHT % [Ref. 6]

C	Mn	P	S	Si	Ni	Cr	Mo	Cu	Nb	Al	N
.04	.90	.006	.003	.25	3.50	.60	.60	1.60	.025	.030	.010

#### **B. HSLA-100 ALLOY DESIGN**

The design of high-strength, low-alloy (HSLA) steels uses several strengthening mechanisms, including grain refinement, precipitation hardening, solid solution strengthening, strain aging, and dislocation substructures produced by phase transformation or deformation processing [Ref. 10]. Since HSLA steels do not rely on a strong martensitic structure for obtaining high strength, very low carbon levels are possible. This low carbon level (0.04 percent) was maintained in the design of HSLA-100 from HSLA-80. The added strengthening was achieved by changing the alloying contents. [Ref.7]

The copper content in HSLA steels acts to retard the  $\gamma$  to  $\alpha$  transformation, allowing the formation of a microstructure containing a high dislocation density. This also leads to an increased supersaturation of copper and micro-alloying elements, in the quenched condition, which in turn permits substantial precipitation strengthening during subsequent aging. The addition of one percent copper can improve the strength of low-carbon steels by as much as 248 MPa [Ref. 11]. This effect is significantly larger than that achieved by solid solution strengthening and accounts for the high copper content in HSLA-100. The potential increase from solid solution strengthening is indicated in Table 2 [Ref. 12]. In marine environments, copper in conjunction with small amounts of other alloying elements (Mn, P, Ni, Cr, Mo, and Si) can significantly improve corrosion resistance [Refs. 11, 13]. Copper additions also reduce hydrogen absorption by forming a stable protective film on the steel surface when the copper content is 0.3 percent or more [Ref. 13].

Nickel increases the toughness of the alloy and reduces the potential adverse effect of copper on the hot working properties of the steel by modifying the ferrite matrix [Ref. 2]. Nickel is also a strong austenite former and suppresses the formation of polygonal ferrite. [Refs. 7, 14]

Chromium and molybdenum influence the precipitation kinetics of copper during cooling, providing for more copper to remain in solution [Refs. 7, 14]. It is speculated that this effect results from the

TABLE 2

**INCREASE IN MPA DUE TO THE ADDITION OF  
EACH WEIGHT PERCENT OF ALLOY [Ref. 13]**

Element	Yield Strength	Tensile Strength
C	+4600	+6800
N <sub>f</sub>	+4600	+6800
P	+670	+670
Sn	+140	0
Si	+85	+85
Cu	+39	+9
Mn	+32	+28
Mo	+11	+45
Ni	0	+9
Cr	-30	-28
Al	0	0

suppression of the  $\gamma$  to  $\alpha$  transformation temperature rather than a large change in the diffusion coefficient. The addition of these two elements make the precipitation hardening response more predictable, which reduces the thickness effect on the amount of increase in the strength. These homogeneous through thickness properties are achieved by altering the CCT diagram to permit slower cooling rates which result in a more uniform cooling of thick plates during processing. Chromium also assists in corrosion protection, while molybdenum in conjunction with niobium promotes acicular ferrite formation. [Ref. 15]

Manganese strengthens the ferrite matrix, controls grain size, and enhances the precipitation hardening mechanism. [Refs. 3, 7, 12]

Grain refinement is further accomplished by the addition of small amounts of niobium. Niobium combines with carbon and nitrogen in

the austenite to form carbo-nitride precipitates. These precipitates suppress recrystallization and grain growth, reducing the final ferrite grain size. Niobium carbo-nitrides also precipitates in the ferrite during and after transformation, which provides further structural refinement and some precipitation strengthening. The fine grain size strengthens and toughens the material and decreases the ductile to brittle transition temperature. [Refs. 2, 7, 10, 12, 14, 16]

The additions of nickel, molybdenum, and manganese lower the transformation temperature, resulting in a finer bainitic microstructure in all plate gauges. The low-carbon bainitic microstructure produces a broader bainitic transition range at lower temperatures, uniform through thickness properties, and in weldments a HAZ with excellent strength and toughness. An increased hardenability enables the bainitic HAZ microstructure to maintain its strength and hardness upon thermal cycling. [Ref. 3]

### **C. ROLE OF COPPER**

The phase boundaries in the Fe-C system are affected by the presence of additional alloying elements, which in turn affect the transformation characteristics on cooling. Copper is one of the alloying elements which, due to its low solubility in ferrite, can be used as a major strengthening element. The substantial precipitation strengthening potential and the synergistic influence on the austenite to ferrite transformation have produced a new family of copper precipitation strengthened steels with:



- a. high yield strength (600–700 MPa),
- b. low transformation temperatures,
- c. good formability characteristics at low temperature,
- d. intrinsic weldability,
- e. excellent corrosion resistance,
- f. fatigue resistance, and
- g. resistance to hydrogen embrittlement

which result in reduced costs.[Refs 4, 16]

The iron-rich portion of the Fe-Cu phase diagram (Figure 1) illustrates the solubility of copper in iron, its decreasing solubility with temperature, and clearly demonstrates why it has such excellent precipitation characteristics. From Figure 1 it can be seen that the copper has a solubility of 2.1 percent at 850° C in ferrite, whereas the amount of copper which can remain in solution falls to 0.35 percent or less at room temperature. [Ref. 15]

During the aging process, the particles which originally nucleate lack contrast in the electron microscope. This is due to their small size, the similarity of the diffraction patterns of the coherent precipitates and iron, and the negligible strains produced by the precipitates due to the small difference in atomic radii ( $\Gamma_{\text{Cu}}/\Gamma_{\text{Fe}} = 1.003$ ) [Ref. 17]. In the early 1960s, Hornbogen and Glenn suggested that the initial strengthening of the Fe-Cu alloys is caused by the formation of coherent copper clusters. In Hornbogen's model of precipitation, two types of particles were identified to contribute in the precipitation process:

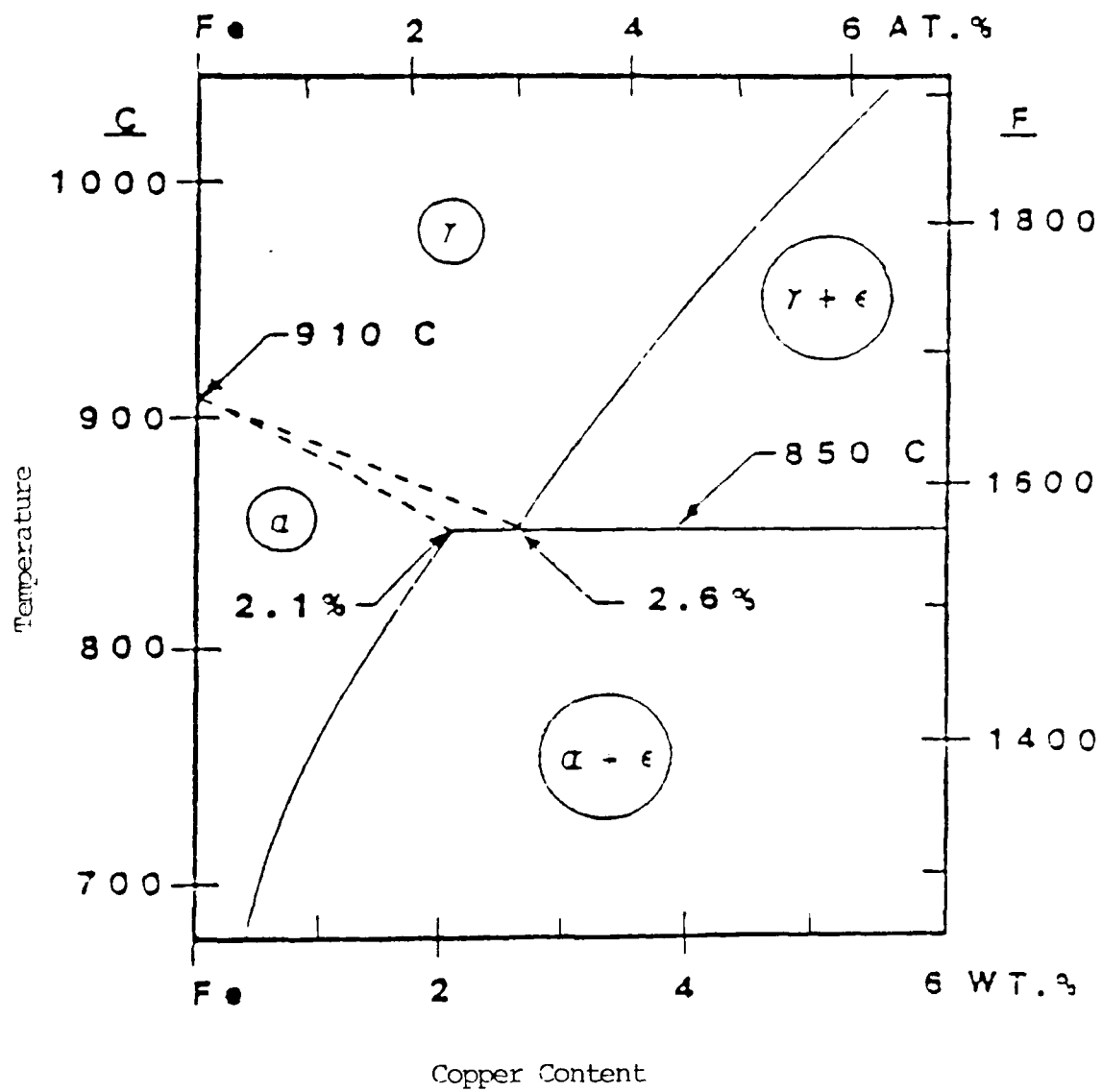


Figure 1. Iron Rich Portion of the Fe-Cu Phase Diagram [Ref. 15]

coherent spherical particles predominant at the early stage and non-coherent rod shaped particles predominant in the overaged condition. [Refs. 17, 18, 19]

In subsequent work on copper precipitation, Speich and Oriani confirmed that the equilibrium shape of the particle is that of rods with hemispherical caps. This shape results from the large anisotropy due to the very poor atomic fit at the ends of the particle, which contrasts with the excellent atomic fit along the cylindrical rods. They also observed that these copper rods have a Kurdjumov-Sachs orientation relationship,  $[01\bar{1}]_{\text{Cu}} \parallel [111]_{\text{Fe}}$  and  $(111)_{\text{Cu}} \parallel (01\bar{1})_{\text{Fe}}$ , with the matrix and their axis are parallel to  $\langle 111 \rangle_{\alpha}$ . This relationship is frequently found for the fcc to bcc martensitic transformation in iron based alloys. [Ref. 20]

In the early 1970s, copper precipitation in iron was studied in detail by Goodman, Brenner, and Low using field ion microscopy. They observed that coherent, copper-rich clusters formed in ferrite during aging and grew by bulk diffusion. These bcc clusters contained less copper than the equilibrium fcc epsilon phase which eventually forms from these clusters upon further aging. The maximum strength was reached while the precipitates were still bcc with an average diameter of 24 Å and an average copper content of 40 to 60 percent. The number density of precipitates remained nearly unchanged until the maximum strength was reached and then decreased during overaging. [Refs. 21, 22]

Copper is considered to be a mild austenite stabilizing element because it slightly lowers the allotropic and Ms temperatures. The beneficial consequence of this effect is the ability to obtain a structure of high dislocation density over commercially feasible cooling rates. This imparts a high basic strength to the matrix. [Ref. 11]

The grain size observed in HSLA-100 copper-precipitation strengthened steel is relatively fine and can be considered the main microstructural feature. The strengthening is realized from a combination of the bainitic microstructure, dislocation density, copper precipitation, and solid solution strengthening. The competing reactions of these strengthening mechanisms make this fine-grain-sized matrix insensitive to the variation of heat treatment. Recovery (lowering the strength) takes place by the rearrangement and annihilation of dislocations, while the precipitation of copper increases the strength. The mechanical behaviour of the alloy is determined by the size and volume fraction of copper-rich precipitates which are the most sensitive to temperature. This is a direct result of the gradual decrease of the hardness profile after aging the alloy to its maximum strength. The length of time the material retains this hardness is a function of temperature and time, but the time can be of considerable length, as seen in Figure 2. [Refs. 22, 23]

#### **D. STRESS-RELIEF CRACKING**

The thermal cycle of the weld process results in residual stresses being left in the weld. The consequence of this thermal cycling

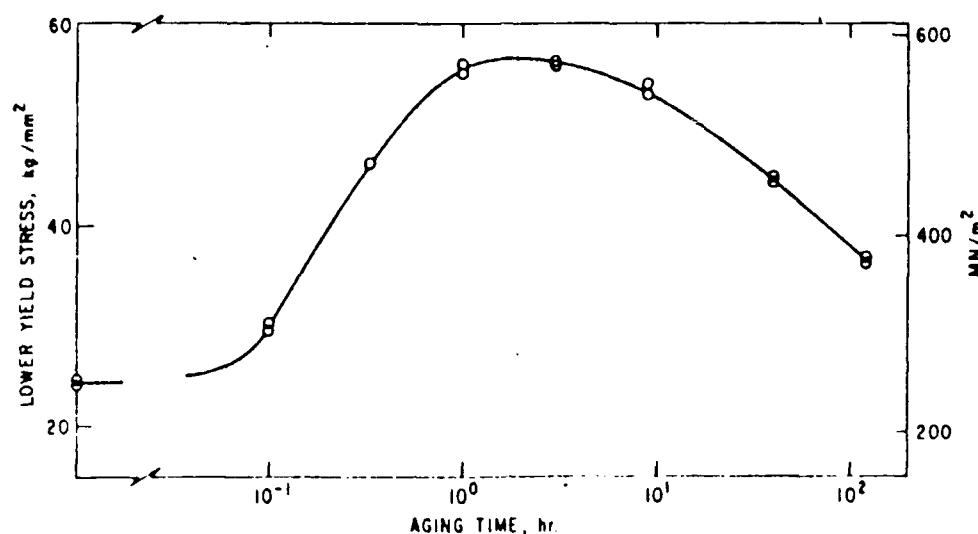


Figure 2. **Yield Stress of Fe-1.4 percent Cu as a Function of Aging Time at 500° C [Ref. 21]**

increases in complexity in weldments which involve multiple-pass welding [Ref. 24]. The responsible factors for these residual stresses are (1) a sharp temperature gradient in the weldment, (2) variation of the flow strength and dimensions of the base and weld metal with temperature, (3) the progressive or step-wise deposition of the joining metal, and (4) the volume changes accompanying transformation of the metal during solidification. As a general rule, the magnitude of the residual stresses increases with the thickness and strength of the plate being welded [Refs. 24, 25]. After cooling to ambient temperature, the weldment may contain residual stresses comparable to the yield strength of the metal at the final welding temperature. [Ref. 26]

The thermal relief of residual stresses is achieved by heating the weldment to a high enough temperature to reduce the yield strength to a fraction of its magnitude at room temperature. The inability of the

steel to sustain the residual stress level causes the initiation of plastic deformation to relax the stresses. Additional relaxation can occur by creep action if heating is continued. Figure 3 illustrates the amount of stress relaxation as a function of time and temperature. A Larson-Miller parameter,  $P$ , has been developed to describe the relaxation of residual stress by creep as a function of time and temperature. It is given as

$$P = T(C + \log(t)) \quad \dots \quad (1)$$

where  $T$  is the absolute temperature of heating (degrees K),

$t$  is the time at temperature in hours, and

$C$  is a constant approximately equal to 20.

The parameter  $P$  has an inverse relationship with residual stress; therefore, a large value of  $P$  is desired. As illustrated in Equation 1, temperature has a much stronger effect than time on stress relief. [Ref. 26]

The linear thermal expansion coefficient of iron at 20° C is  $11.7 \times 10^{-6}$  per °C [Ref. 27]. This represents a measurable expansion at the temperatures experienced during the welding thermal cycle, resulting in the potential for a large residual stress. Although post-weld heat treating is capable of relieving residual stress, it is difficult to remove the stresses associated with thermal expansion.

Stress-relief cracking is defined as the intergranular cracking which predominantly occurs in the coarse-grained HAZ during

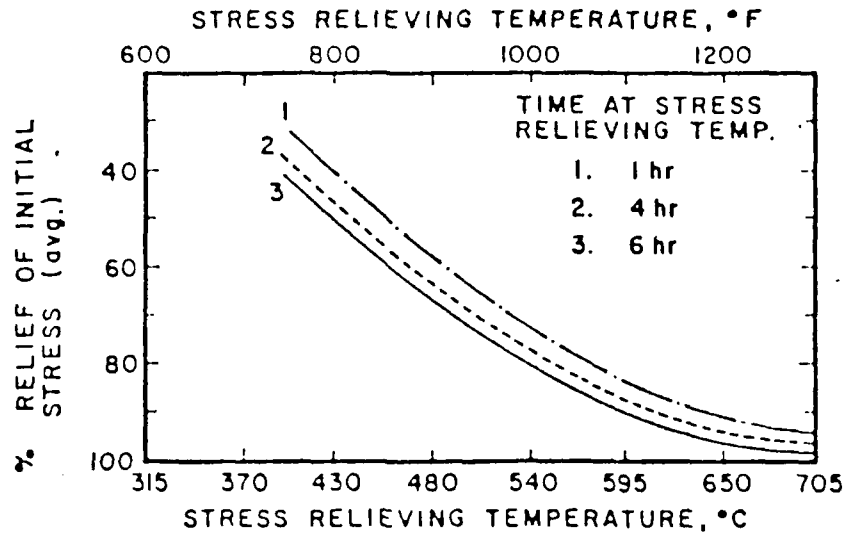


Figure 3. **Stress Relief in a Carbon Steel** [Ref. 26]

exposure of the weldment to thermal relief. This phenomenon can occur because the conversion of residual elastic stresses by a process of creep relaxation into permanent strain can lead to cracking when the creep deformation is permitted to concentrate in the narrow heat-affected zone [Ref. 28]. The occurrence of stress-relief cracking in 2.25CR-Mo-V and Mn-Mo-Ni steels has been attributed to a finely dispersed intragranular precipitate, molybdenum or vanadium carbides. These carbides strengthen the matrix, which transfers the creep strain to the grain boundary [Ref. 29]. This restricts grain boundary sliding and migration, creating intergranular voids which result in a loss in creep ductility and increased notch sensitivity [Ref. 30]. The presence of alloy/impurity elements such as chromium, molybdenum, vanadium, copper, sulfur, phosphorus, arsenic, antimony, aluminum, and tin at the grain boundaries serves to further restrict the amount of

grain boundary deformation that can be accommodated without cracking [Ref. 4]. Stress relief cracking has been documented to occur in the 500°-650° C temperature range and has been a problem in those materials which are capable of precipitation through the formation of alloy carbides. [Refs. 5, 31]

Recently studies have, on the basis of fracture appearance, identified two different modes of stress relief cracking. At a low stress relief temperature (400° to 600° C) and high stress, a low ductility intergranular fracture (LDIGF) mode has been observed. The fracture surface associated with LDIGF is a surface characterized by smooth intergranular facets. The transition from this mode to the other is a function of temperature and stress. At higher stress relief temperatures (>600° C) and low stress, the fracture is by an intergranular microvoid coalescence (IGMVC) mode. The fracture surface is characterized by dimples, formed on the grain boundaries, which are speculated to be due to the coalescence of individual creep cavities. [Refs. 5, 29, 32, 33]

Considerable work has been conducted at various research facilities utilizing Gleeble Simulation and/or the Lehigh Restraint method on the cracking susceptibilities of various low-alloy steels. However, the behaviour of HSLA-80 and HSLA-100 steels is relatively unknown.

Recent research by Lundin, Menon, and Chen has demonstrated the susceptibility of ASTM A710 (HSLA-80) to stress-relief cracking in the 560° to 680° C temperature range. They have postulated that the susceptibility of this steel to stress-relief cracking is probably related



to the intragranular precipitation of copper-rich particles, which in turn leads to grain matrix strengthening and concomitant strain accumulation in the prior austenite grain boundaries. [Ref. 4]

Okada, et al. have shown that 0-1.6 percent copper can improve the toughness of the fusion line and the HAZ as long as no aging is applied. Their explanation for the improvement in toughness attributed it to the refinement of microstructure caused by a change from upper to lower bainite [Ref. 11]. Recent study at Lehigh University has also shown that stress relieving does not soften the heat-affected zone close to the fusion line, but may increase the hardness because reprecipitation can occur in the solution-treated regions. This was observed to be especially true in low heat input welds. [Ref. 32]

Throughout the literature, the emphasis has been on the realization that the incidence of stress-relief cracking in a steel can be reduced by changing the welding parameters to minimize the size of the coarse HAZ. Small weld beads limit the grain coarsening and increase toughness by reheating the underlying heat-affected zone. A low angle of attack on the work piece and low bevel angle preparations also reduce the risk of reheat cracking [Ref. 33].

#### **E. WELDING OF HSLA-100 STEEL**

The primary advantage of using HSLA-100 steel as a replacement or substitute for HY-100 steel is based upon achieving a significantly reduced fabrication cost by eliminating or reducing preheat requirements and interpass temperature restrictions. [Refs. 1, 3, 7, 8, 9]

HY-100 exhibits excellent strength, fracture toughness, and resistance to stress corrosion cracking in sea water. However, it requires expensive welding procedures to produce acceptable properties in weldments. The HAZ produced in HY steels is a hard martensite structure, which is subsequently tempered by the heat of the following passes in a multipass joint. The primary reason for welding preheat is to prevent underbead cracking in the hard martensitic HAZ of HY steels [Ref. 3].

The HAZ of the HSLA steels are ferritic or low-carbon bainitic microstructures which do not harden or soften, because the heat of welding causes dissolution of the copper. Such microstructures do not require preheat and are not susceptible to hydrogen-assisted cracking. This can be attributed to the low carbon content, as illustrated in Figure 4. Post-weld heat treatment is reported to increase the strength while reducing the toughness of the HAZ due to the precipitation strengthening of the alloy. [Ref. 3]

#### **F. FILLER METAL/ELECTRODE**

Welding consumables specifically for welding HSLA-100 have not been developed. In welding and weldability tasks in the HSLA-100 certification program for submarine non-pressure hull structure, all welding was preformed using HY-100 qualified consumables, MIL-120S wire electrode for spray gas metal-arc welding (GMAW-S). The welding and weldability testing conducted by DTNSRDC have not resulted in heat-affected zone cracking. However, the strength and

		C	Mn	P	S	Si	Cr	Ni	Mo	Cu	Cb	V	B	CE*
TRADITIONAL NAVY STRUCTURAL STEELS	HY 80	.16	.26	.01	.01	.25	1.40	2.70	.40	.05	—	.01	—	0.78
	HY 100	.17	.25	.01	.01	.25	1.40	2.90	.40	.05	—	.01	—	0.81
CURRENT DEVELOPMENT HSLA (CONV. ALLOY)	HSLA 80	.04	.55	.01	.005	.30	0.70	0.90	.20	1.20	.04	—	—	0.50
	HSLA 100	.04	.90	.01	.005	.25	0.60	3.50	.60	1.60	.03	—	—	0.81

\*C E. = CARBON EQUIVALENT

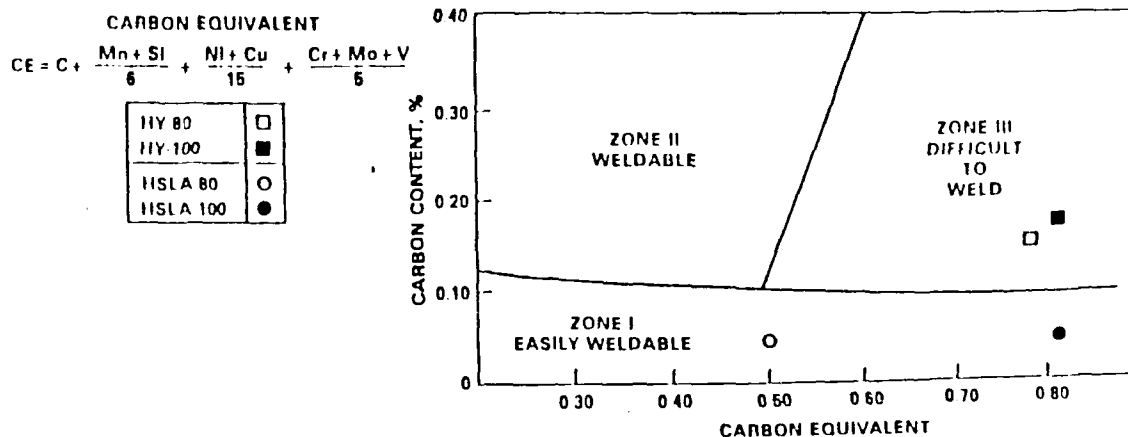


Figure 4. Granville Diagram—Chemical Composition, Carbon Equivalents, and Weldability for HY-80, HY-100, HSLA-80, and HSLA-100 Steels

toughness deficiencies observed in some HSLA weldments appear to be due to the inherent limitations of the welding consumables employed. [Ref. 3]

The microstructure of the HY-100 weld metal with a GMAW-S process is typically acicular ferrite. This microstructure is a randomly

oriented arrangement of short ferrite plates which form within the austenite grains in an interlocking nature.

## **G. APPLICATIONS**

When HSLA-100 is substituted for a lower-strength steel, as the Navy is considering, costs will be decreased in several areas. The increased strength levels allow the use of thinner plates, which will reduce the overall weight of the ship. The amount of welding consumables and manhours would be reduced because the number of required passes would be decreased. The thinner materials are easier to weld without preheat, which results in additional costs savings. In addition, the thinner material translates into longer plates from the mill, which means fewer joints required per unit item.

Potential surface ship applications have emerged where HSLA-100 may replace HY-series steel with large fabrication cost reductions. These are: aircraft carrier structures (CVN), aircraft carrier magazine side protection systems (CVN/CV), flight deck and other structures of the LHD-1 class, and submarine-non pressure hull structures.

### III. EXPERIMENTAL PROCEDURE

#### A. MATERIAL

A welded plate measuring 560 x 305 x 25 mm was received from David Taylor Naval Ship Research and Development Center (DTNSRDC) for study of its susceptibility to stress relief cracking. The plate had been welded using a spray Gas Metal Arc (GMAW-S) process, perpendicular to the rolling direction, with a double bevel 60° joint. The weld consisted of 12 passes, with each pass receiving a heat input of 2.17 kJ/mm. Figure 5 illustrates the weld bead sequence and lists the actual welding parameters. The chemical composition of the base metal and electrode are given in Table 3.

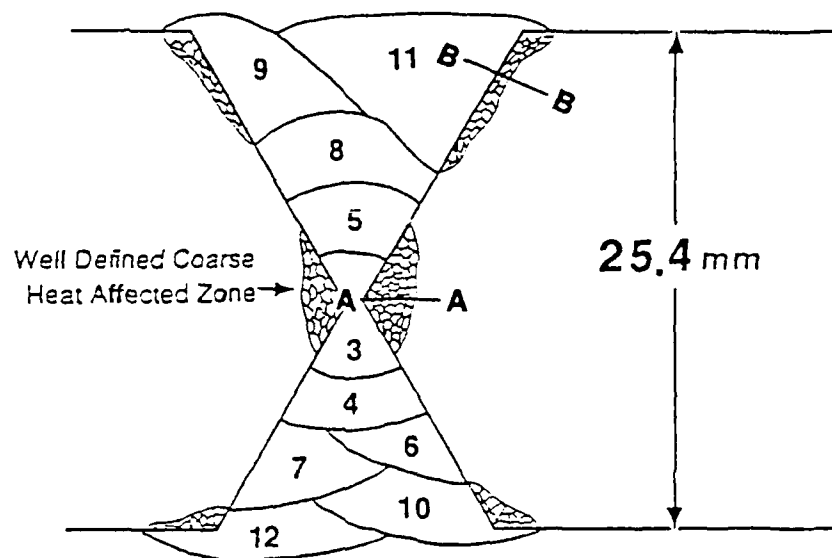
TABLE 3

CHEMICAL COMPOSITION OF  
THE BASE METAL AND ELECTRODE

	C	Mn	P	S	Si	Cu	Ni	Cr	Mo	Al	Cb	Zr
Base Metal	.04	.86	.004	.002	.27	1.58	3.55	.57	.60	.032	.030	--
Electrode	.07	1.54	.007	.005	.36	0.01	2.28	.29	.47	.02	--	.01

#### B. SAMPLE PREPARATION

The steel was cut perpendicular to the weld direction to give a 6 mm thick sample from the center of the plate. The sample was then cut on both sides of the weld and prepared for microscopic



#### WELDING PARAMETERS

Base Metal: HSLA-100

Process: Gas Metal Arc Welding— Spray

Electrode: 120S-1

Electrode Handling: As Received

Preheat Temperature: None

Interpass Temperature: 15° to 121° C

Voltage: 26 Volts

Amperage: 300 Amps

Travel Speed: 216 mm/min

Heat Input: 2.17 kJ/mm

Figure 5. **Weld Bead Sequence and Welding Parameters**

examination using standard metallographic techniques. The polished surface was etched for approximately eight minutes using a two-percent Nital solution in order to reveal the sequence of weld passes and the location of the HAZ. Figure 6 is a macrostructure of the as-received weldment. Microhardness measurements were taken across the HAZ and correlated to the corresponding microstructure. Optical and Transmission Electron Microscopy were used to characterize the microstructure along the traverses and throughout the HAZ.

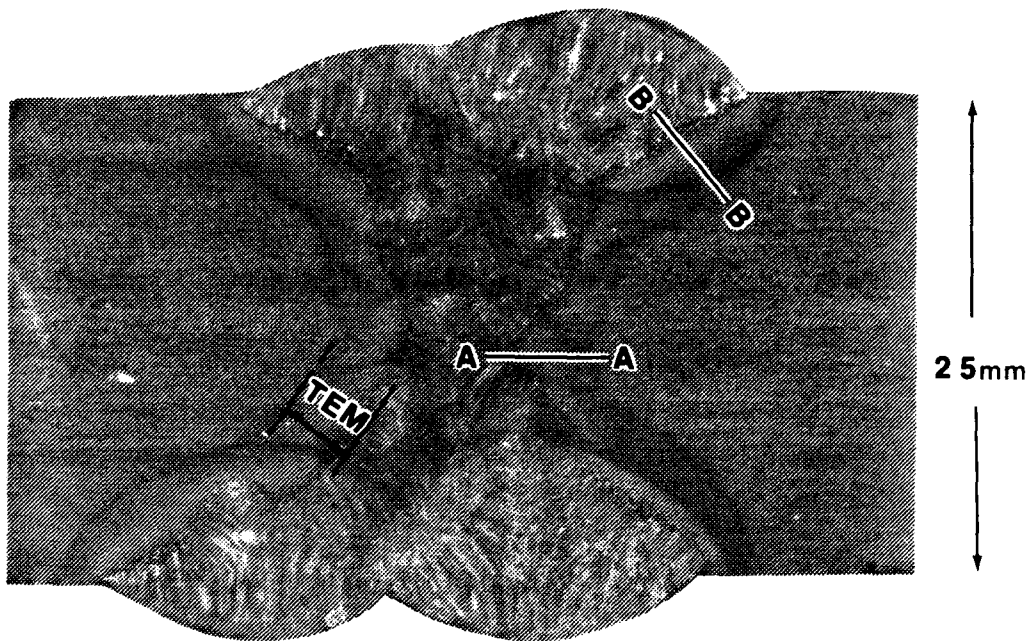


Figure 6. **Macrostructure of the Weld Passes and HAZ**

The remainder of the plate was sectioned perpendicular to the weld direction, parallel to the first cut, to produce 6 mm thick slices for cutting flat tensile specimens. The weld was located in the center of the gauge length, as illustrated in Figure 7. The tensile specimens

were lightly etched using a two-percent Nital solution for approximately 10 seconds to highlight the location of the weld metal and the HAZ. Thermocouples were spot-welded to the weld metal, fusion line, and HAZ. A copper induction coil was positioned around the gauge length of the specimen, which was then inserted into the specially designed grips. The weldment was tested for stress-relief cracking using a Materials Test System (MTS) and Cycle Dyne Induction Heater.

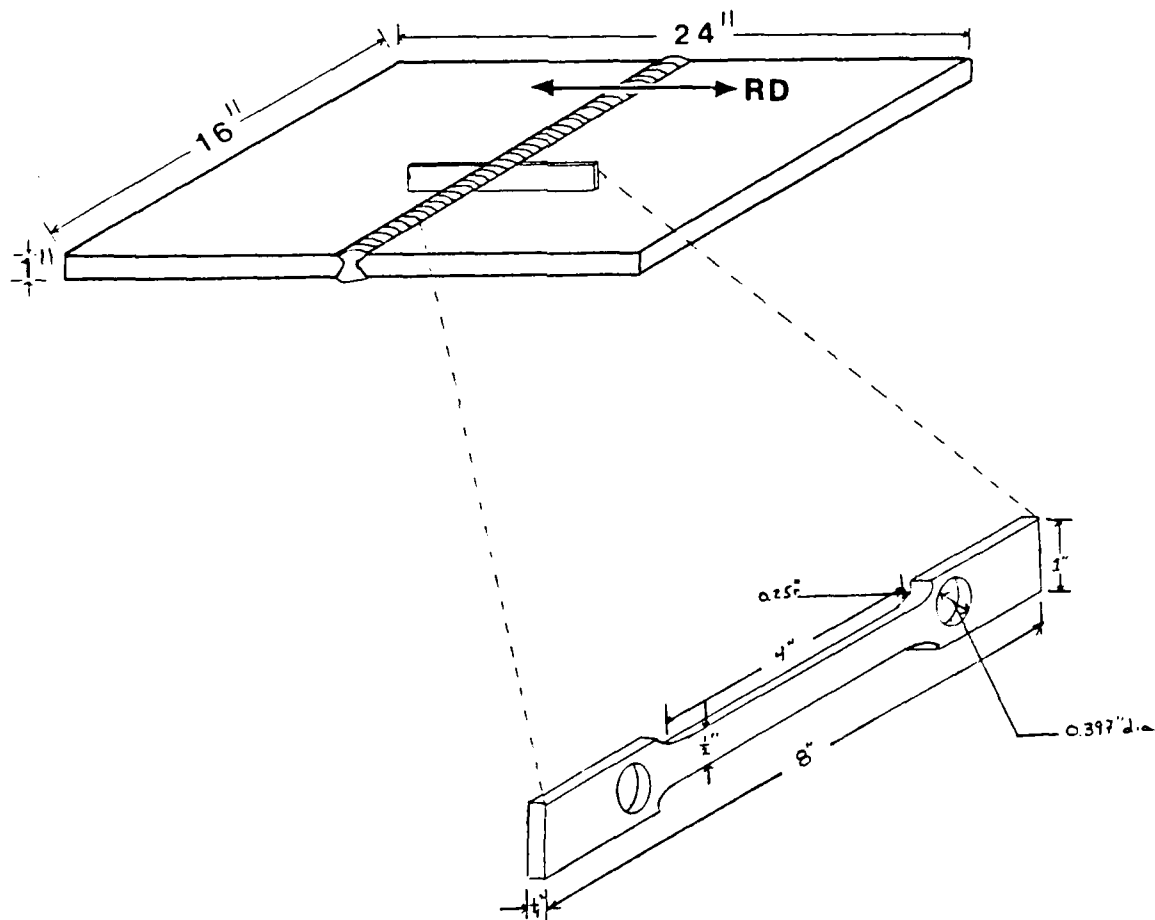


Figure 7. Plate and Tensile Specimen Dimensions



### **C. MICROHARDNESS MEASUREMENTS**

The as-received weldment was etched with two-percent Nital for approximately 30 seconds to highlight the weld metal and HAZ. A diamond scribe was used to mark a 10 mm line perpendicular to the fusion line, extending from the weld metal to the base metal. This was used as a guide for the microhardness traverse. A Buehler microhardness tester was used with a 300 gram load to obtain the Vickers hardness measurements. The spacing between indentations was 0.1 mm near the fusion line and 0.2 mm spacing further out into the HAZ and base metal.

Microhardness measurements were taken near the center of the 60° bevel (traverse AA) and on the last weld pass (traverse BB) of the as-received metal as indicated in Figure 6. In addition, microhardness measurements were taken on the center of the bevel in tensile specimens which had been stress relieved for an hour (traverse CC). All microhardness traverses spanned the HAZ over a length of 5 to 7 mm.

### **D. OPTICAL MICROSCOPY**

The microstructure along the microhardness traverse was also examined with a Zeiss Universal Research Photomicroscope. A series of micrographs was taken at selected locations to correlate the microstructure associated with the different regions and hardness along the traversed line. All micrographs were taken at a magnification of 500x. The grain size and lath widths were measured in the coarse HAZ using the intercept method at 500x magnification.

#### **E. SCANNING ELECTRON FRACTOGRAPHY**

Fracture surfaces of the tensile specimens were examined with a Cambridge Stereo Scan S4-10 scanning electron microscope (SEM) operated at 40kv. The fractured specimens were cut to an appropriate size using a hack saw to minimize the amount of corrosion which may have occurred from wet cutting.

#### **F. AUGER ELECTRON SPECTROSCOPY**

Two of the fracture surfaces were sent to Naval Weapons Center China Lake for Auger analysis. They were both heated to 650° C after being loaded to approximately 220 MPa. One of the samples failed upon heating while the other was stress relieved for one hour (see Testing Procedure).

#### **G. TRANSMISSION ELECTRON MICROSCOPY**

The TEM specimens were prepared by making an initial cut in the base metal region, parallel to the fusion line as shown in Figure 6. An ISOMET Low Speed Wafering Machine, using a diamond wheel, made the first cut at the fusion line. Subsequent cuts were made 0.25 mm apart, passing through the HAZ into the base metal. Nine wafers were required to traverse the entire HAZ in the as-received metal.

The wafers were then hand sanded, with 600 grit emery paper, to a thickness of 0.15 mm. They were then lightly etched using two-percent Nital to highlight the weld metal from the HAZ and unaffected base metal. At selected locations, 3 mm diameter discs were punched

and further thinned using 600 grit emery paper to a thickness of 0.08 mm. Final thinning was accomplished using a Struers Tenupol electropolishing apparatus. The electrolyte was maintained at 13° C and consisted of 10 percent perchloric acid and 90 percent glacial acetic acid. The power supply was maintained at 50-60 volts, resulting in a current of 180-200 milliamps. The thin foils were examined using a Jeol-120 CX transmission electron microscope operated at 120kv.

#### **H. TEST APPARATUS**

A Material Test System (MTS) 810 apparatus was used in conjunction with a Cycle Dyne Induction Heater and a Hewlett-Packard Data Acquisition System. A Hewlett-Packard strip recorder was used to record the stress changes and ram position.

On the MTS, the loading is provided via a hydraulic actuator and grip assembly. The load cell and stroke output voltages were calibrated for each test. The output was monitored digitally and plotted on the strip recorder.

A 3 mm copper tube was used to manufacture an induction coil by shaping the copper tubing to a machined block or rod and then covered with an insulating material. The ends of the coil were then flanged and fastened to the insulated conducting lines of the induction heater. The insulated coil was placed around the gauge length of the tensile specimen and centered to ensure heating was directed towards the weldment. A plastic holding block was designed and manufactured to mount the induction heater to the MTS. This arrangement ensured that the coil remained stationary during heating and

provided an insulated barrier to the MTS. This was an important consideration because it eliminated any possibility of creating a field around the support arm of the load cell or a short to the tensile specimen. The temperature application and sustainment were accomplished with the use of a MTS Model 409 Temperature Controller.

The Hewlett-Packard Data Acquisition System was used to record the temperatures of the thermocouples mounted on various locations of the tensile specimen. A Basic software program was used to record the temperatures from 15 different thermocouples during testing. This program was capable of recording a reading from each of the 15 thermocouples every second.

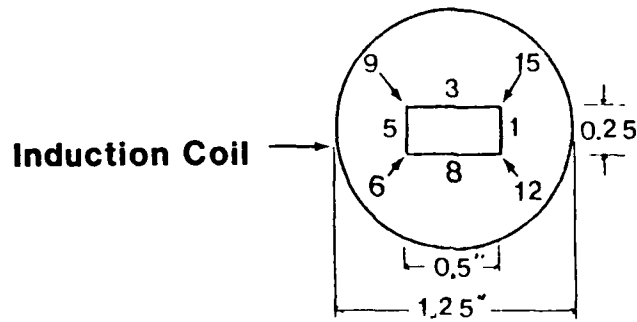
Owing to the high temperatures involved, a grip assembly had to be designed and manufactured to match the existing water-cooled equipment. An AISI 52100 steel stock was selected for the designed part to be machined because of its excellent machinability in the normalized condition and its superior response to heat treating. The machined grips were heated in an argon atmosphere to the austenitizing temperature of 855° C , martempered in hot oil (200° C), and subsequently tempered in an argon atmosphere at 550° C to obtain a final hardness of 36 RC [Ref. 34]. It was important to obtain this strength to ensure that the grips could safely carry the applied loads. The grips were designed such that they attached to an existing mount which was capable of being connected to a supply of flowing cold water. This configuration was used to prevent the grip assembly from heating up and possibly stress relieve with the tensile specimen.

## **I. TEMPERATURE MEASUREMENT AND CONTROL**

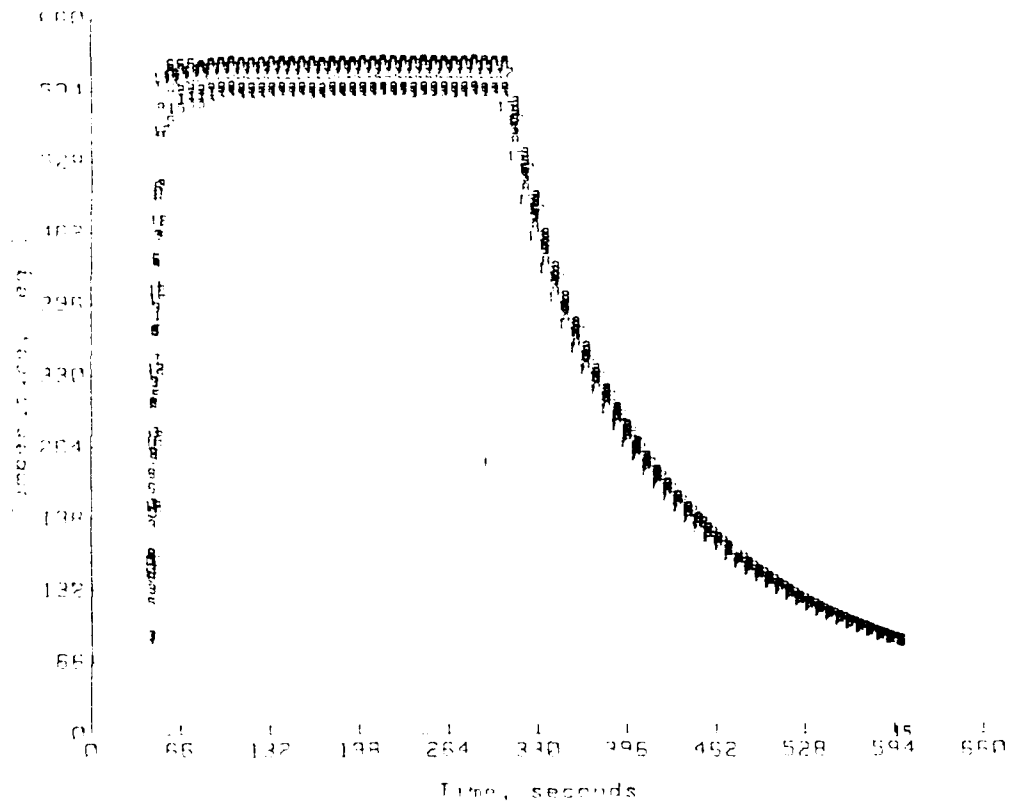
Temperature measurement was accomplished using chromel/alumel thermocouples which are useful over the temperature range  $-200^{\circ}$  to  $1300^{\circ}$  C. All thermocouples were tested in an ice-water bath ( $0^{\circ}$  C), warm water, and boiling water ( $100^{\circ}$  C), and all indicated the correct temperatures. This verified the calibration of the digital reader and the data acquisition system.

Thermocouples were spot-welded to a specimen to determine the temperature variations around and along the gauge length of the tensile specimen at different nominal temperatures. The copper tubing was shaped in rectangular, square, and circular configurations, tested, and compared to find the optimum conditions to produce a uniform temperature in the specimen center. The distance from the surface of the tensile specimen to the coil was also varied with changes in the coil size and shape. The smaller coils exhibited a more uniform heating profile, but little distinction could be made between the temperature profiles due to the shape of the coil. The temperature difference between the edge corners and the flat surfaces of the specimen were negligible, regardless of the shape of the induction coil tested. A circular induction coil, with a 30 mm inside diameter, was selected because it gave the desired temperature profiles around and along the specimen length and was the easiest to center around the gauge length.

Temperature profiles for this circular coil, with time, are shown in Figure 8. Figure 8A shows the temperature changes with time in

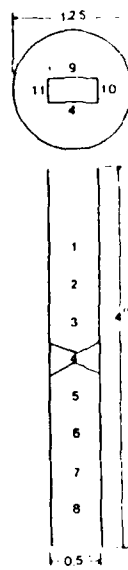


Thermocouple Placement on the Test Specimen in the Induction Coil

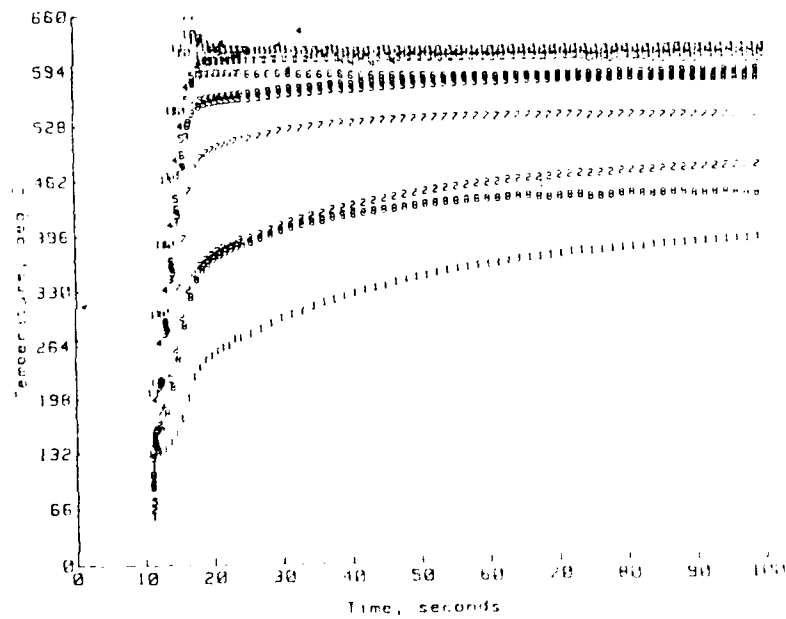


Note the small temperature gradient maintained throughout the test.

Figure 8A. Temperature Changes With Time in Several Locations Around a Cross-Section of the Specimen



Thermocouple Placement on the Specimen in the Induction Coil



Note the small temperature gradient in the center of the gauge length.

Figure 8B. **Temperature Changes Along the Specimen**

several locations around a cross-section of the specimen. Note that a very small temperature gradient was maintained throughout the heating-up, stress-relieving, and cooling-down periods. Figure 8B shows the temperature changes along the specimen. Note the small temperature gradient in the central portion of the gauge length (i.e., thermocouples 3, 4, 5, 6, 9, 10, and 11).

#### **J. TESTING PROCEDURE**

Each tensile specimen was lightly etched in two-percent Nital for approximately 10 seconds to highlight the HAZ. Thermocouples were spot-welded to the HAZ, fusion line, and weld metal. A circular induction coil was centered around the gauge length and then attached to the loading system of the MTS. The testing apparatus is illustrated in Figure 9. The thermocouples had to be checked to ensure that they had not come loose upon mounting the specimen. The cooling systems were activated to cool the grip assembly and the induction coil. Upon confirmation that all recorders were operating, the specimen was loaded at a strain rate of  $4.23 \times 10^{-4}$  mm/(mm s) to a desired stress level, line AB (Figure 10). The MTS was transferred to load control on reaching the desired stress level, point C (Figure 10), and the specimen was then heated to the test temperature, point D (Figure 10). The switching of the system to load control removed the effect of thermal expansion during heating on the applied stress. After a stable test temperature was reached, in about 30 seconds, the MTS was returned to stroke control locking the crosshead in a stationary



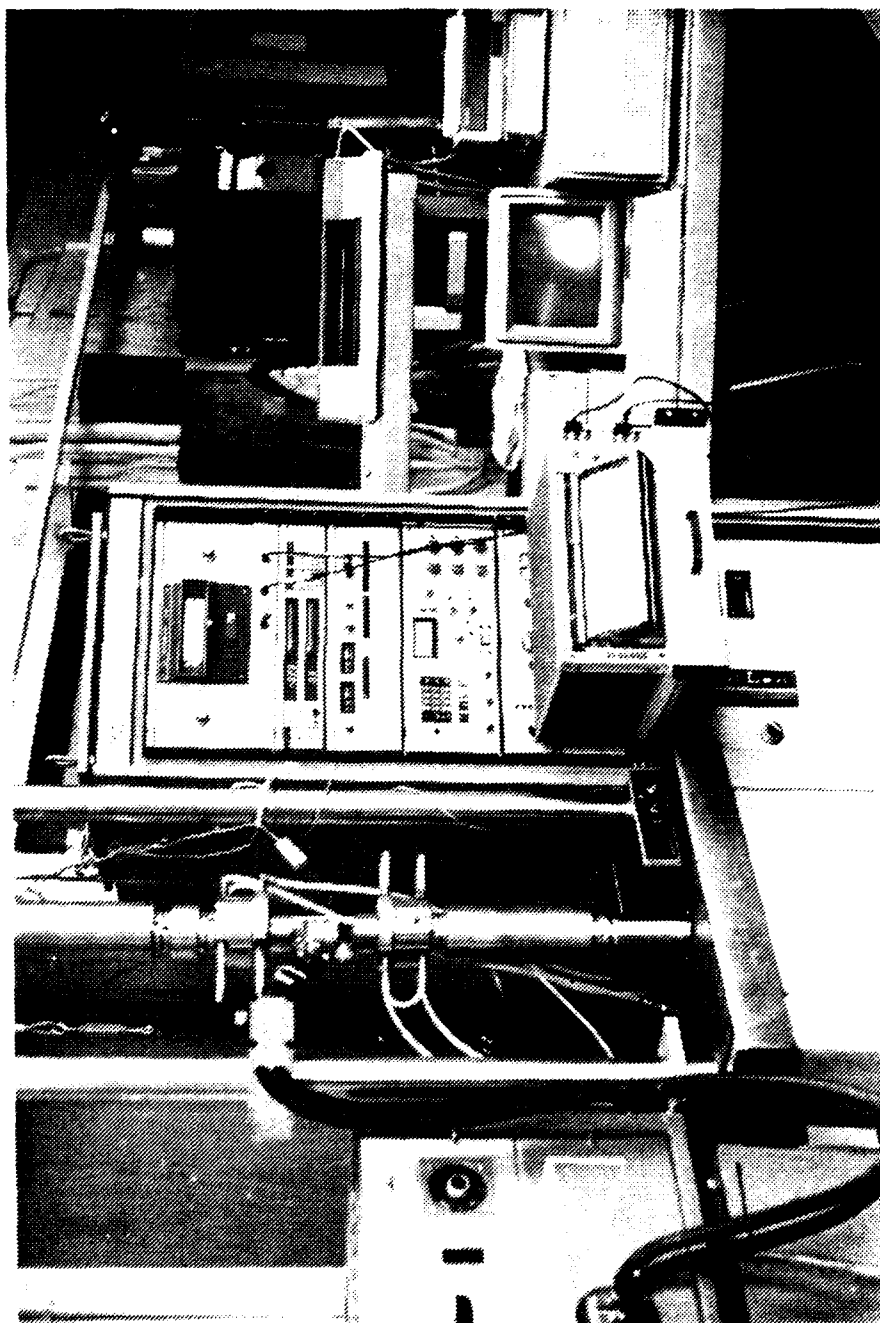


Figure 9A. Testing Apparatus

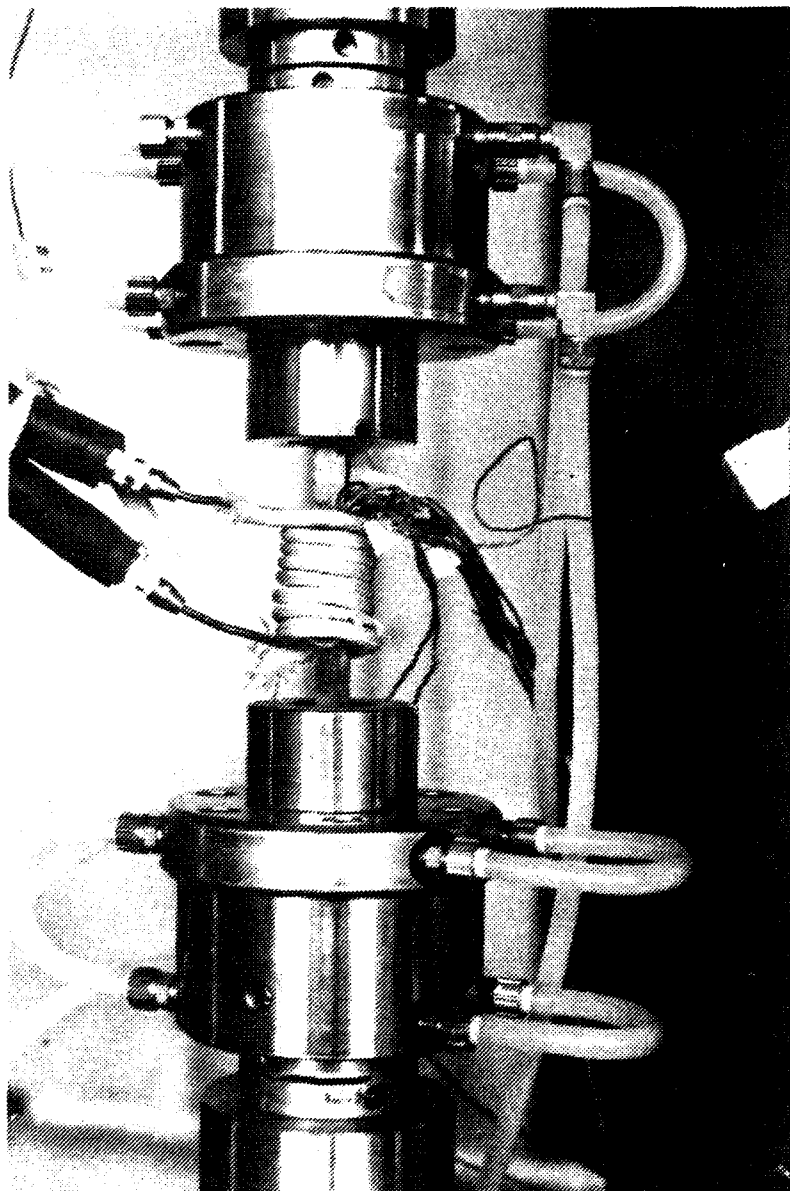


Figure 9B. **Testing Apparatus—Grip Assembly**

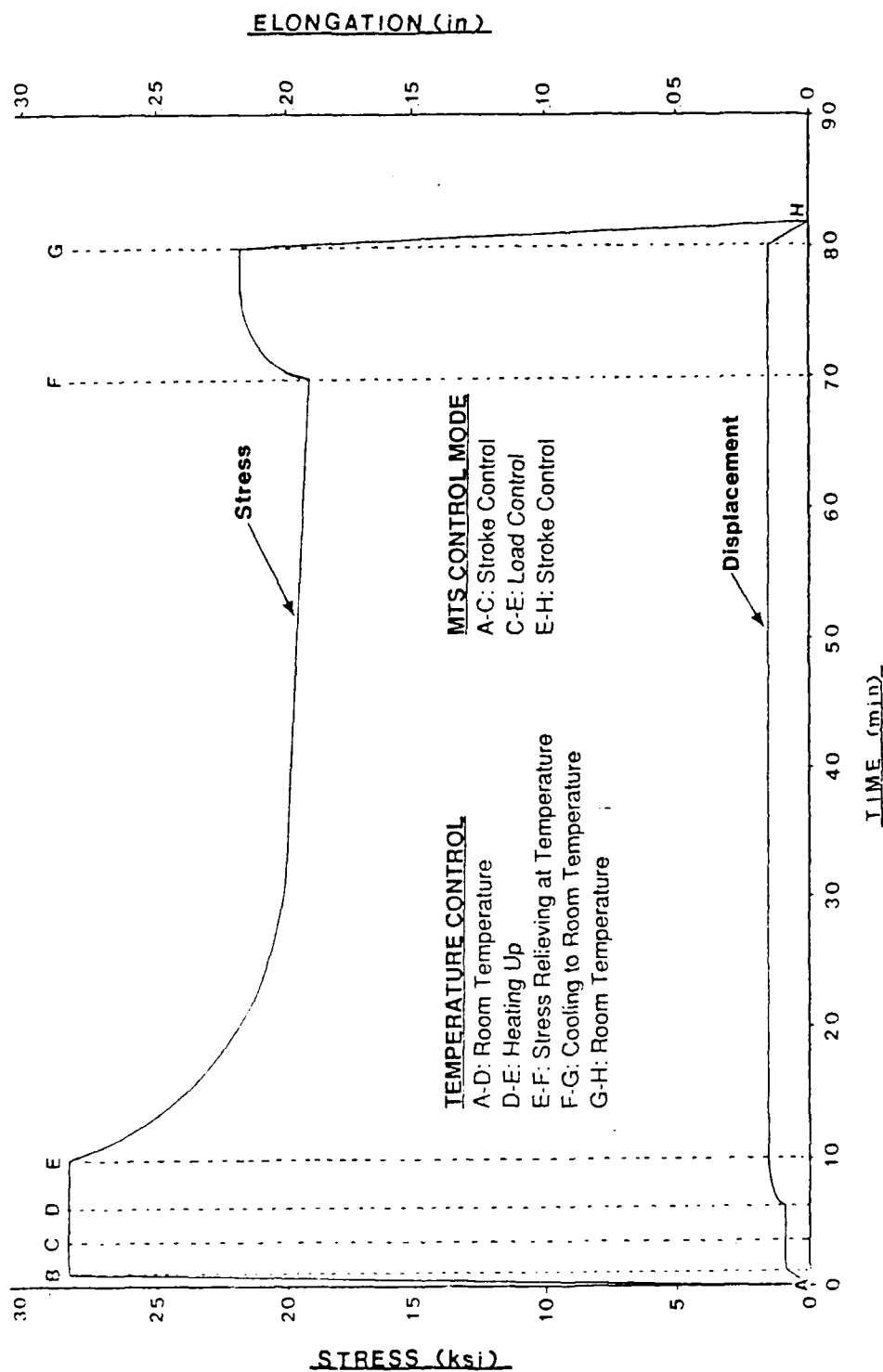


Figure 10. Stress Relaxation Schematic of the Testing

position, point E (Figure 10). Stress relieving was conducted for a maximum period of one hour. The specimen was allowed to cool for 10 minutes to room temperature, points F to G (Figure 10). The load was removed using the same strain rate as used in initial loading, points G to H (Figure 10), and the test specimen was removed from the MTS.

The sample was polished, etched, and optically examined for surface cracks. After photographing any observed cracking, the specimen was pulled to failure and the fracture surface was examined through the Scanning Electron Microscope. Transmission Electron Microscopy foils were then obtained from selected areas and analyzed.

## **IV. EXPERIMENTAL RESULTS**

### **A. MACROSTRUCTURE**

The weld bead sequence of the weldment (Figure 5) shows the pass locations, numbered from 3 to 12. The first two passes were subsequently mechanically removed to alleviate the residual stresses normally associated with the first few weld passes in a double V weldment. The size of the passes increased with pass number and the papillae are larger and more pronounced in the last half of the weld passes.

The welding parameters were consistent for all passes with the exception of the interpass temperature which unintentionally ranged from 15° to 120° C. The size of the HAZ ranged from 4 mm at the center to 2 mm at the surface of the plate. This can be attributed to the different cooling rates and temperatures reached at various locations in the base metal. The average prior austenite grain size in the coarse-grained HAZ in the center of the weldment was measured to be 54 microns. The grain size in the HAZ decreased as the distance from the fusion line increased.

### **B. MICROHARDNESS MEASUREMENTS**

The locations of the microhardness traverses are shown in Figures 5 and 6. The hardness profile across the HAZ for traverse AA (center of the 60° bevel), and BB (last weld pass) are illustrated in Figures 11

and 12. The profile of the two hardness measurements superimposed on one another is shown in Figure 13.

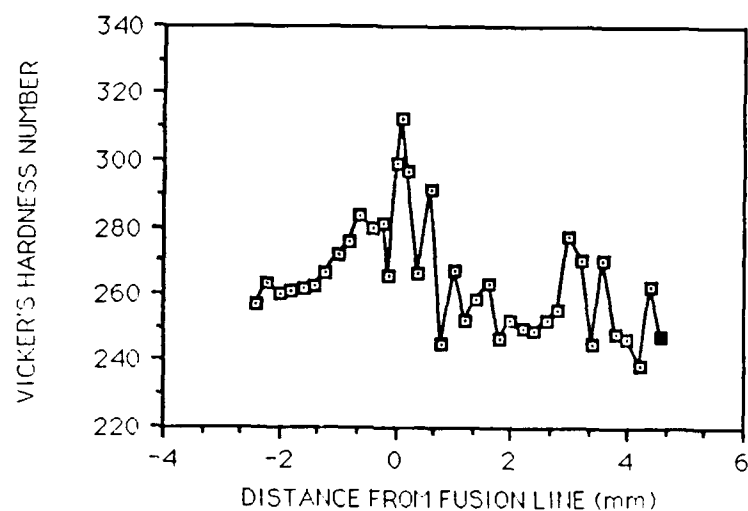


Figure 11. **Microhardness Traverse AA at the Center of the Weldment**

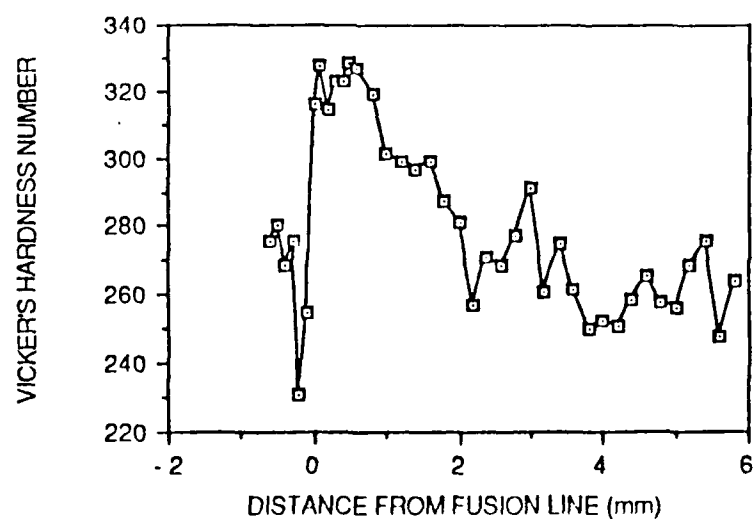


Figure 12. **Microhardness Traverse BB at the Last Weld Pass**

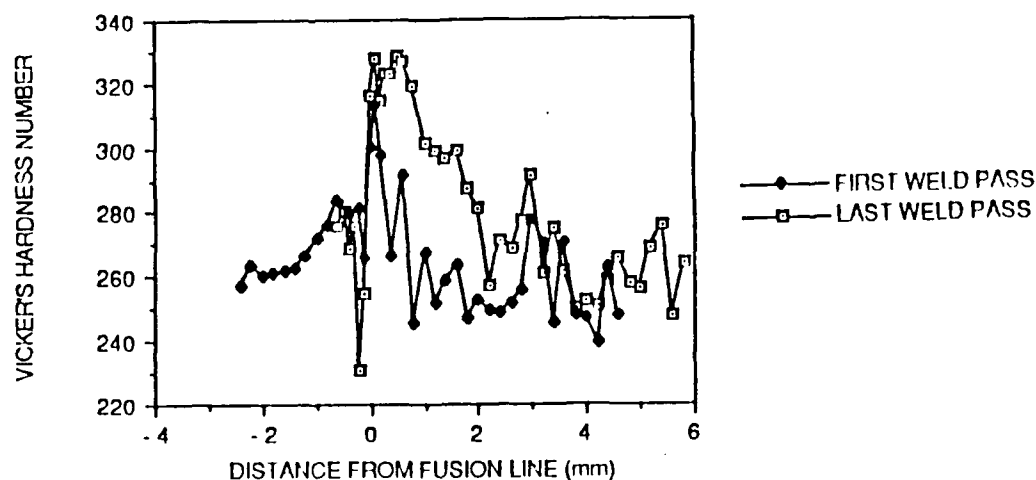


Figure 13. **Comparison of Microhardness Traverse AA and BB**

Traverse AA slightly increases through the weld metal towards the fusion line from a Vickers Hardness Number (VHN) of 260 to 283. At the fusion line there is a drop of 20 VHN, followed by an immediate rise to 320 VHN. The hardness then falls off to a value of 250 at the HAZ/base metal interface prior to a slight increase to an average value of 260 VHN in the base metal.

Traverse BB follows a similar trend except that the discontinuity at the fusion line is much more pronounced. The fall from the maximum hardness of 330 VHN is more gradual than traverse AA, but the hardness averages out to the same 260 VHN in the base metal.

The comparison of the two traverses in Figure 13 indicates that both hardness profiles follow an analogous trend in that they exhibit a sharp discontinuity at the fusion line and both have the same average 260 VHN in the base metal. The only apparent difference is in the HAZ, where traverse BB is slightly harder throughout the entire region.

The hardness profile of CC (center of the 60° bevel after stress relief for one hour at 650° C), is illustrated in Figure 14. It has the same sharp discontinuity at the fusion line followed by a decreasing hardness across the HAZ. A maximum hardness of 328 VHN was obtained in the coarse HAZ and average value of 240 VHN was achieved in the base metal.

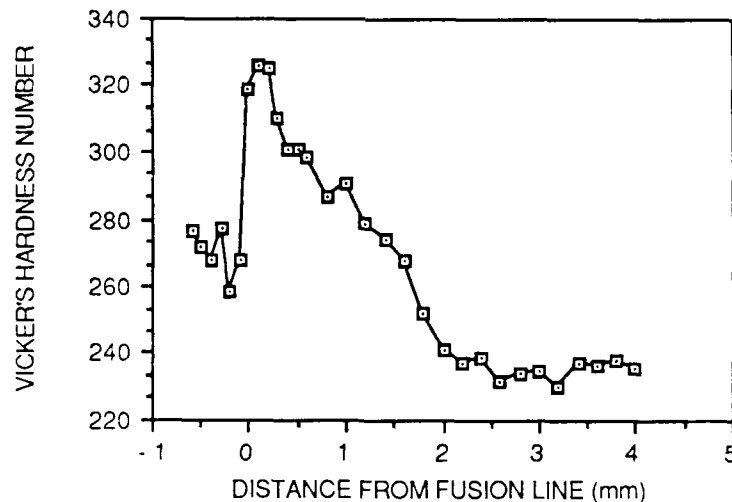
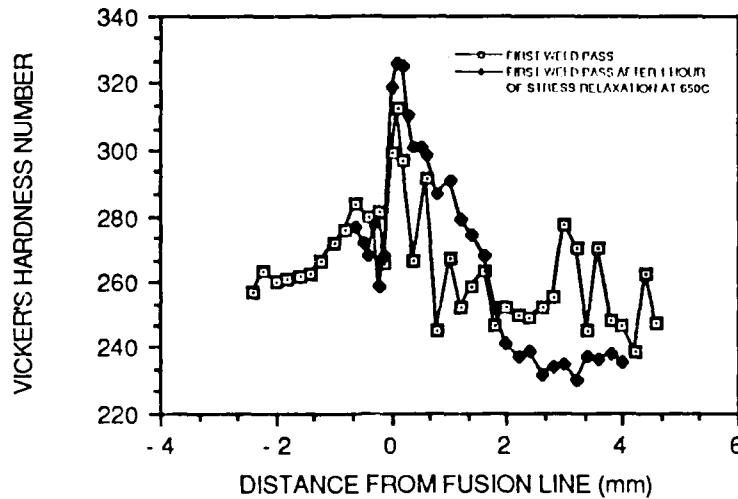


Figure 14. **Microhardness Traverse CC taken at the Center of the Weldment after Stress Relieving at 650° C for One Hour**



The comparison of the hardness profiles of the center of the weldment before and after stress relief is shown in Figure 15.



**Figure 15. Comparison of Microhardness Before (AA) and After (CC) Stress Relief Testing**

The hardness is higher in the coarse-grained HAZ and lower in the unaffected base metal for traverse CC.

Five distinct regions in the hardness profiles of traverses AA and CC were selected for microstructural investigation. These were:

- a. weld metal,
- b. coarse HAZ,
- c. fusion line,
- d. fine HAZ, and
- e. base metal.

## **C. MICROSTRUCTURE IN THE AS-RECEIVED WELDMENT**

### **1. Weld Metal**

The weld metal was predominantly a fine acicular ferritic microstructure with a small amount of polygonal ferrite. Figure 16 shows a microstructure of acicular ferrite. The average prior austenite grain size was measured to be approximately 60 microns in diameter. TEM analysis of the weld metal also revealed a predominantly acicular ferritic structure, Figure 17, with a high dislocation density. Figure 18A and B show some evidence of a twinned martensitic morphology between the ferrite laths. No evidence of copper precipitation was detected.

### **2. Coarse-Grained Heat-Affected Zone**

The coarse-grained HAZ consisted of a low-carbon ferritic/bainitic microstructure. This area contained two distinct regions (Figure 5). The zone in the center and the HAZ at the surface of the plate contained large grains which depicted the prior austenite grain boundaries when etched (Figure 19). The HAZ in between these areas did not show the prior grain boundaries clearly when etched (Figure 20). In both instances the lath morphology was visible. The TEM micrographs further highlight the lath morphology and indicate regions of retained austenite and high dislocation density. The dark field micrographs in Figure 21 illuminates the retained austenite between the lath boundaries. Very fine copper particles were detected in this region only after a careful observation of the dark field (Figure 22B).

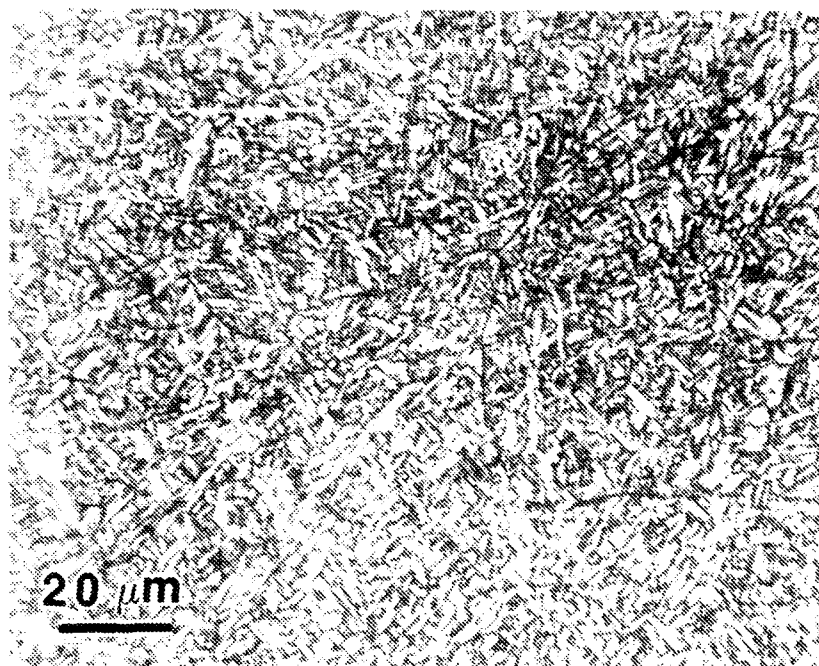


**Figure 16. Optical Micrograph of the Weld Metal in the As-Received Condition Depicting the Fine Acicular Ferrite**

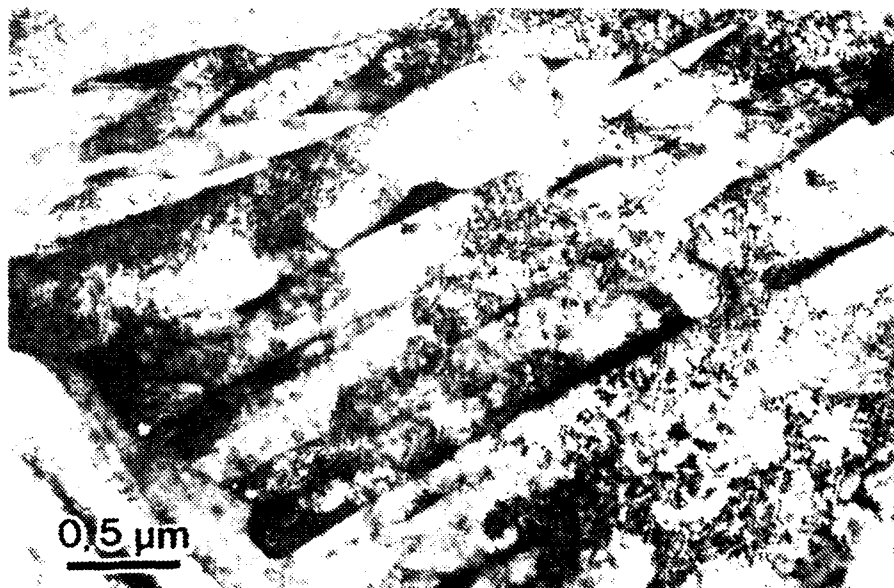


**Figure 17. TEM Micrograph Illustrating the Fine Acicular Morphology with a High Dislocation Density**

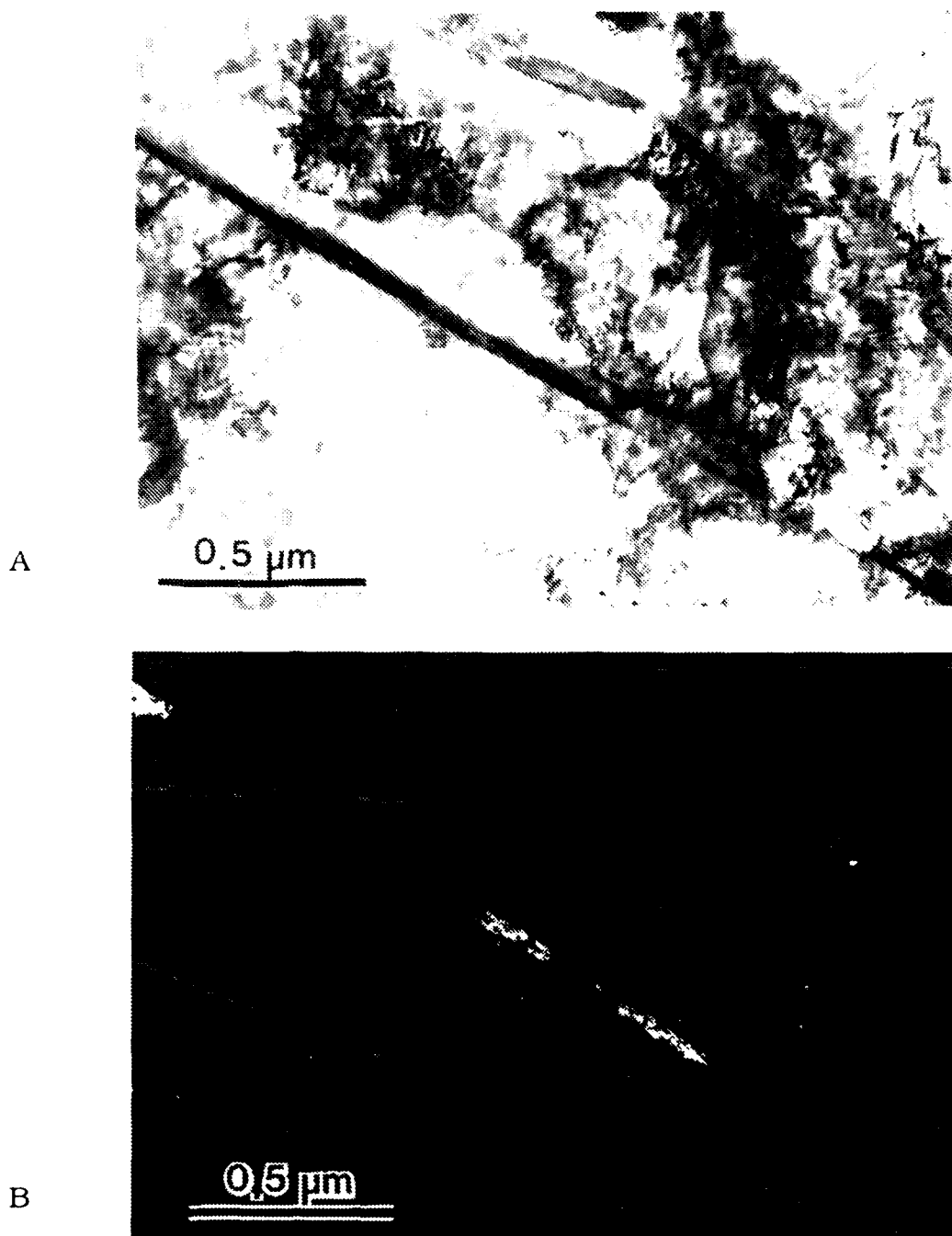
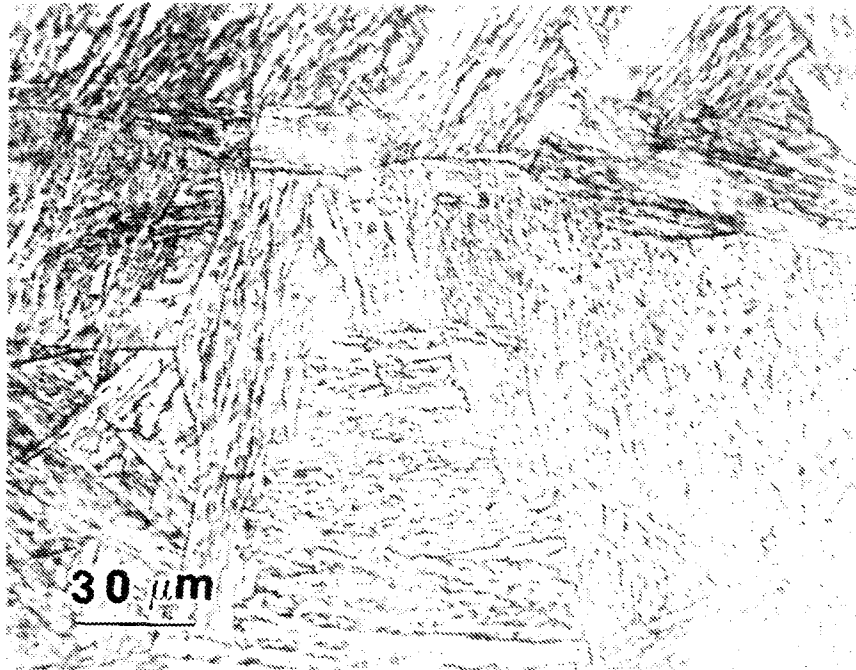
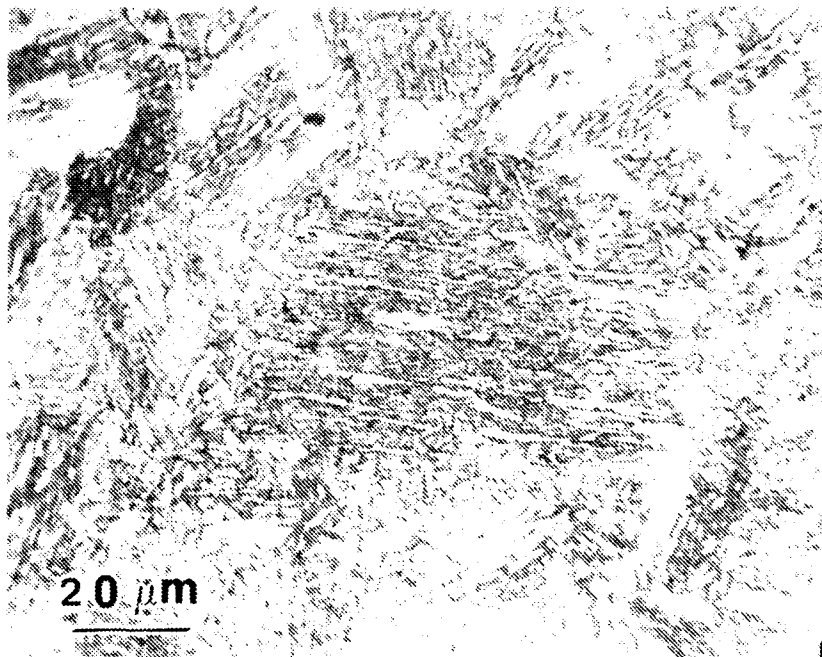


Figure 18. A **Bright Field TEM Micrograph of the Weld Metal Prior to Stress Relief Testing, Showing a Ferritic Structure and Twinning**  
B **Dark Field Illuminating the Twinning in the Same Region**



**Figure 19. Coarse-Grained HAZ Illustrating the Well-Defined Prior Austenite Grain Boundaries**



**Figure 20. Coarse-Grained HAZ Illustrating the Poorly Defined Prior Austenite Grain Boundaries**

A

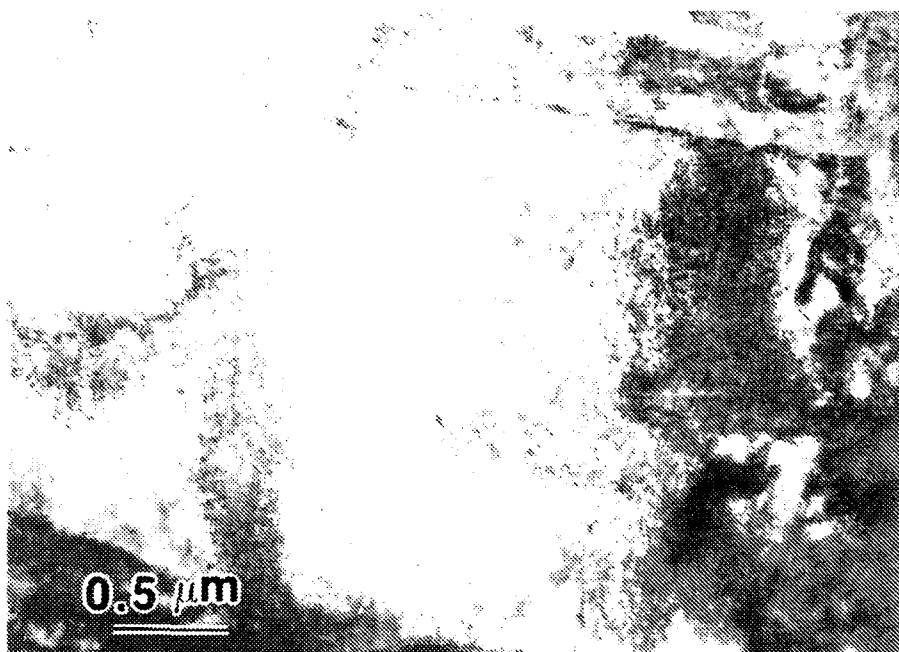


B



Figure 21. A **Bright Field Micrograph Illustrating the Lath Morphology and High Dislocation Density**  
B **Dark Field Micrograph of the Same Area Illuminating the Retained Austenite Between the Laths**

A



B



Figure 22. A **Bright Field Micrograph of a Large Ferrite Grain in the Coarse-Grained HAZ**

B **Dark Field Micrograph of the Same Area Illuminating the Fine Copper Precipitates**

### 3. Fusion Line

The fusion line microstructure was denoted in all instances of a sharp transition from acicular ferrite of the weld metal to the ferritic/bainitic microstructure of the coarse-grained HAZ. Mixing of the weld metal with the base metal was evident on and near the fusion line by the observation of small islands of acicular ferrite adjacent to, but not in the weld metal. Figure 23 illustrates discernable lath packets in the large prior austenite grains.

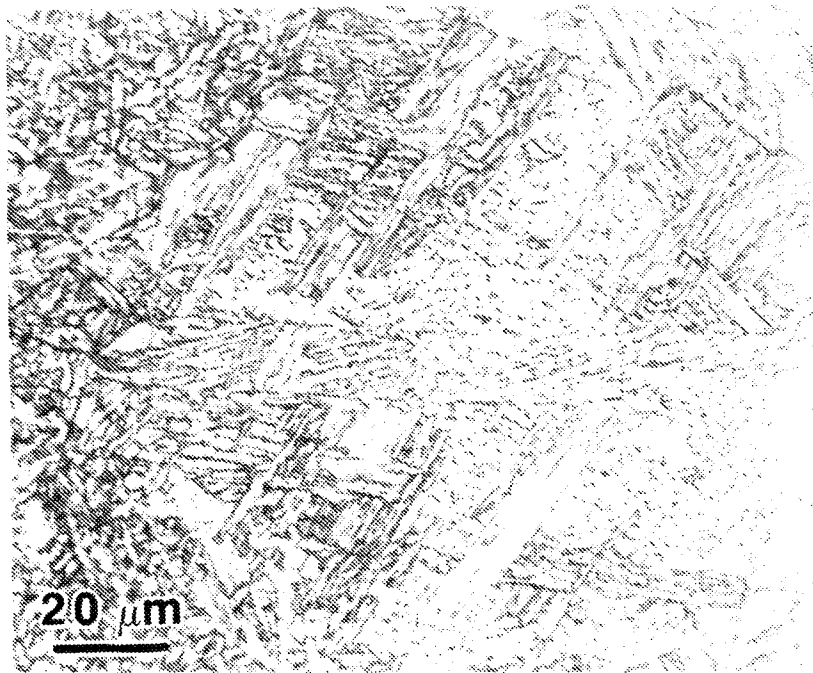


Figure 23. **Optical Micrograph of the Fusion Line at the Center of the 60° Bevel**



#### **4. Fine-Grained Heat-Affected Zone**

The optical micrographs (Figures 24 and 25) indicate a decrease in the prior austenite grain size as the distance from the fusion line increases. Relatively large particles are visible in Figure 25, which shows a uniform distribution. Bright and dark field TEM micrographs (Figure 26A and B) show the presence of large particles of retained austenite inside the ferrite grains.

#### **5. Base Metal**

The microstructure of the base metal (Figure 27) is predominantly lath ferritic/bainitic with large copper precipitates. Throughout this region banding was visible upon etching which ran parallel to the rolling direction. TEM analysis show a lath-like morphology with uniform copper precipitation observed in the matrix and on dislocations. Copper particles on the boundaries were coarser than those observed in the matrix (Figures 28 and 29). Areas containing a high number of dislocations and precipitates suggest an interaction resulting in an increased strength of the alloy. This feature was evident throughout the TEM analysis of the area.

### **D. MICROSTRUCTURE AFTER STRESS-RELIEF TESTING**

#### **1. Weld Metal**

The weld metal was essentially acicular ferrite (Figure 30). TEM analysis showed interlocking laths and some inclusions which are characteristic of an acicular ferrite microstructure.

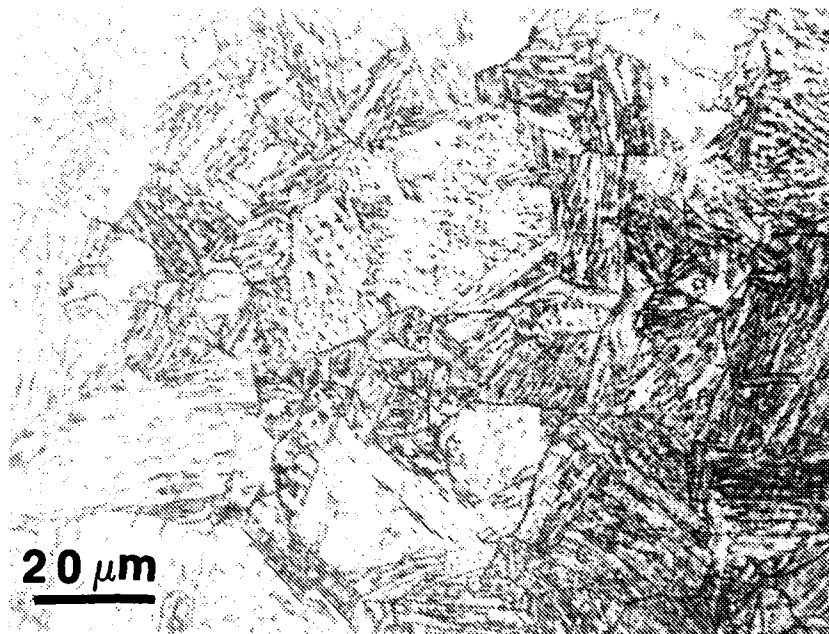


Figure 24. **Optical Micrograph Taken in the Middle of the HAZ**

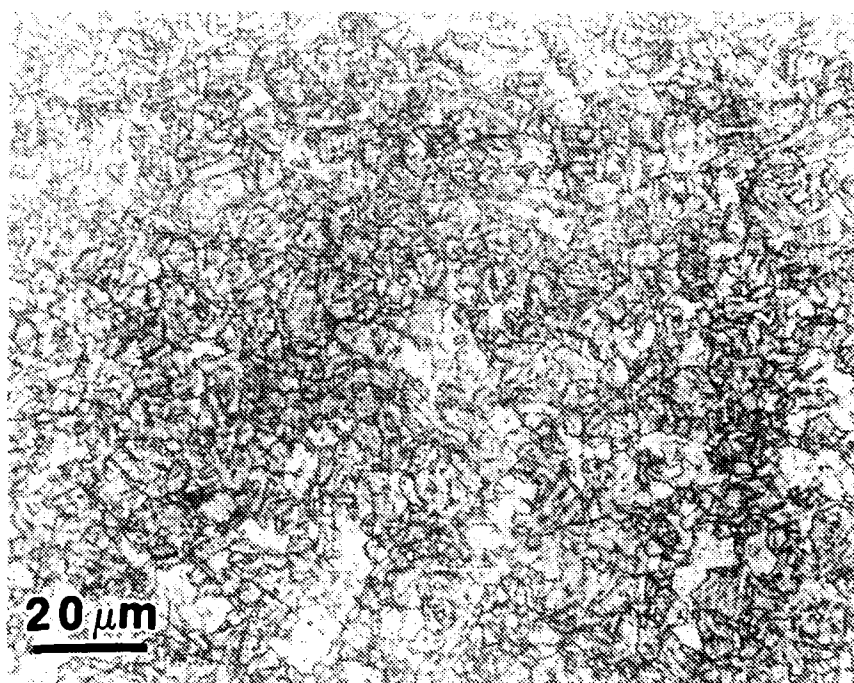
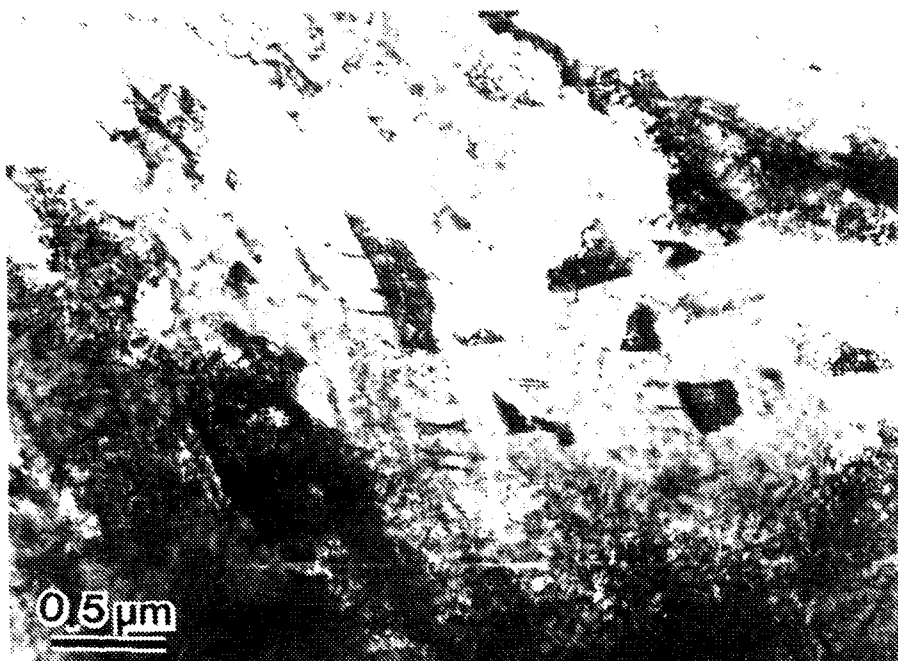


Figure 25. **Optical Micrograph of the Fine-Grained HAZ Illustrating the Decrease in Grain Size from Figure 24**

A



B

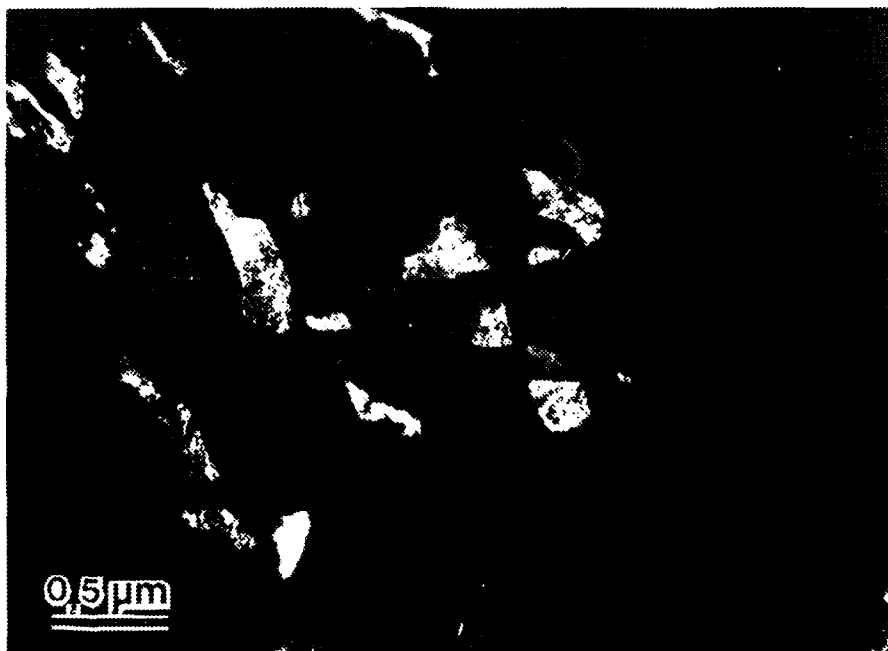
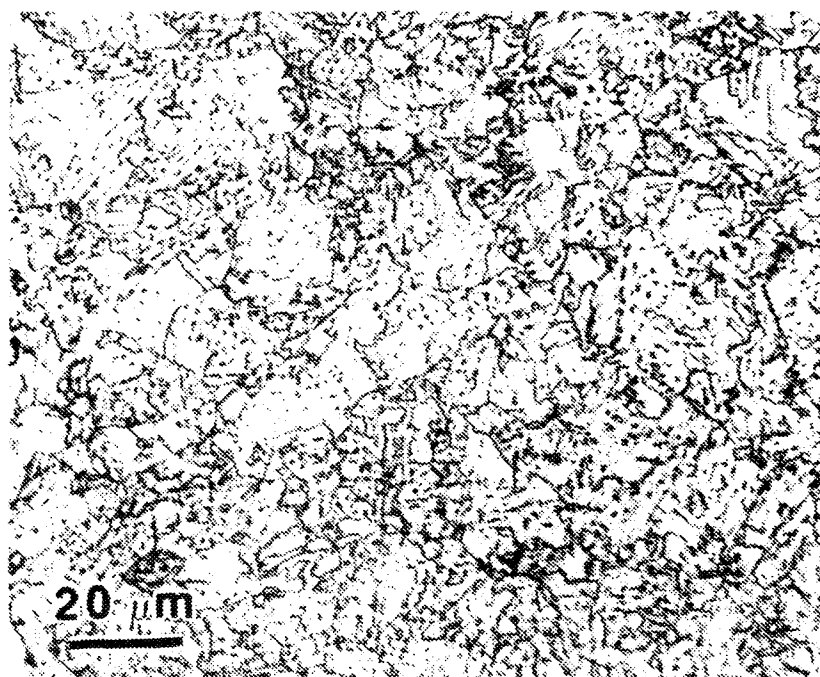
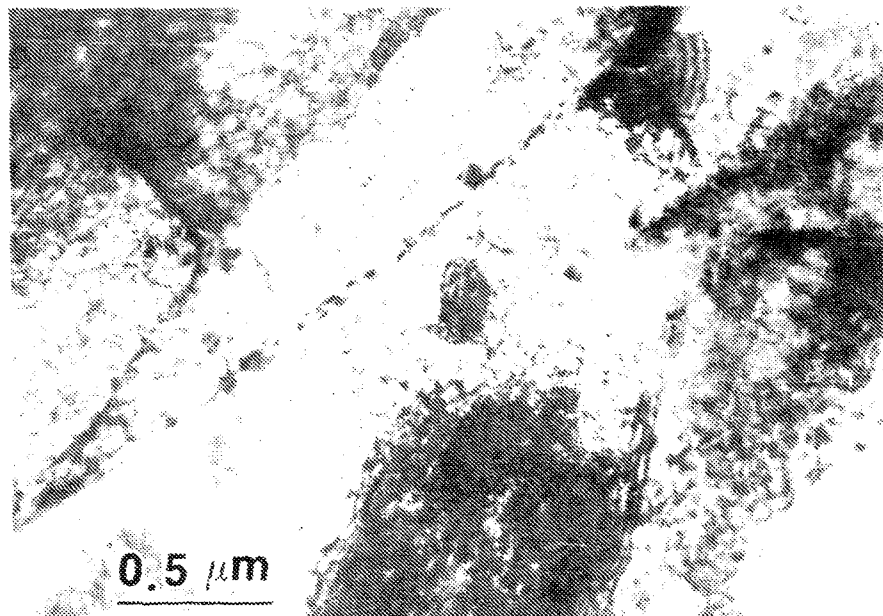


Figure 26. A **Bright Field Micrograph of a Grain in the Fine-Grained HAZ**  
B **Dark Field Micrograph of the Same Area Illuminating the Islands of Retained Austenite Inside the Grain**



**Figure 27. Optical Micrograph of the Base Metal**



**Figure 28. TEM Micrograph Indicating a Lath Morphology in the Base Metal with Larger Copper Precipitates on the Lath Boundaries**

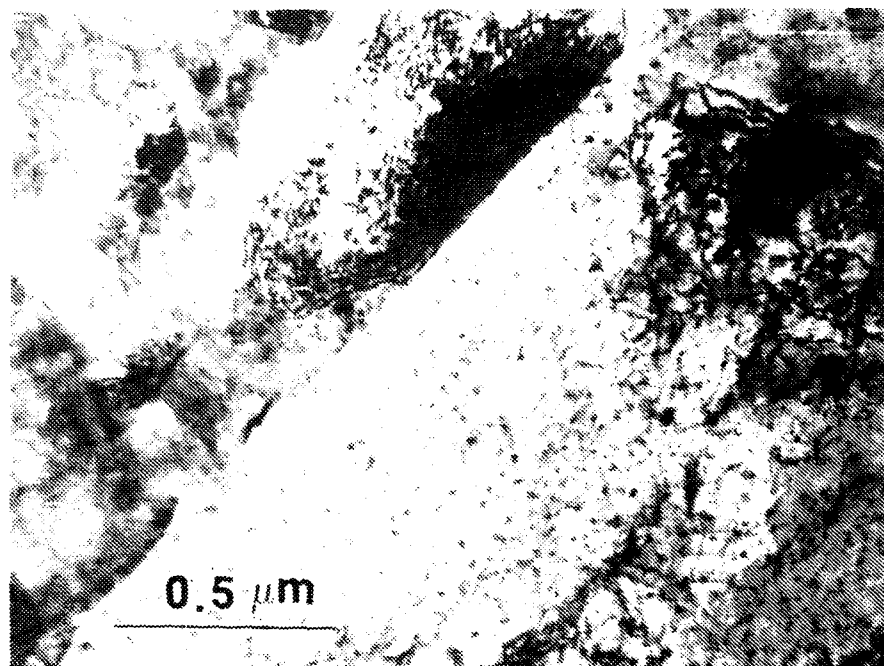


**Figure 29. TEM Micrograph in the Base Metal Illustrating the Dislocated Ferritic Structure with Copper Precipitates**

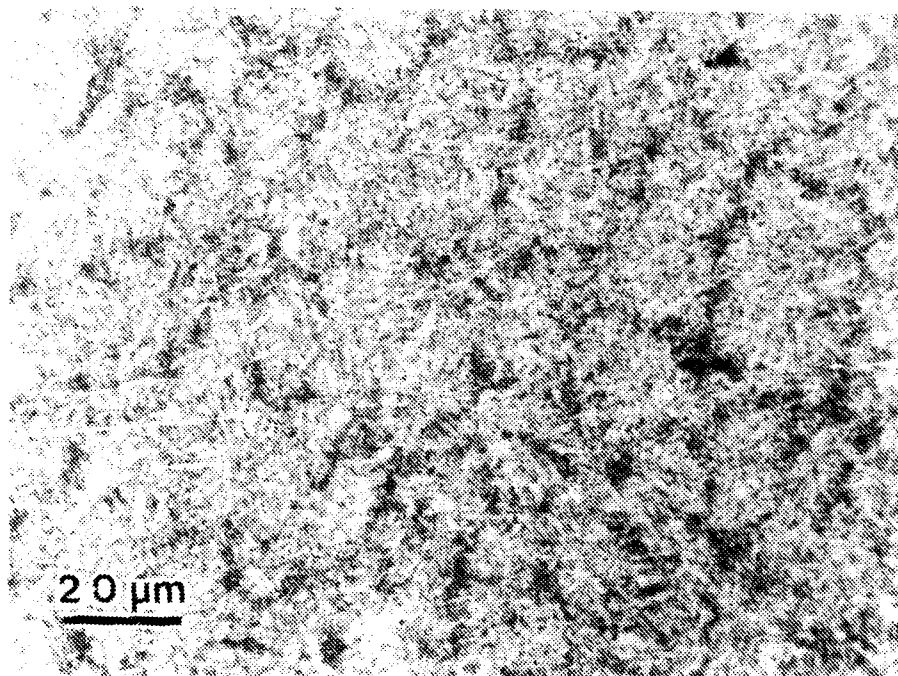


**Figure 30. Optical Micrograph of the Weld Metal After Stress Relieving at 650° C for One Hour**

## **2. Coarse-Grained Heat-Affected Zone**

Optical microscopy showed no significant differences from the as-received coarse-grain HAZ, but TEM analysis of this region indicated that some recovery had taken place (Figure 31) as dislocations tended to polygonalize leading to the formation of small subgrain boundaries. Retained austenite (Figure 32) was now observed between the laths and throughout the observed region. Twinned martensite fragments were occasionally noticed between the laths. Copper precipitates were observed throughout the matrix, with the coarser particles being preferentially located between the boundaries (Figure 33A and B).

## **3. Fusion Line**

This region was a mixture of acicular ferrite and tempered bainite. TEM analysis revealed a ferritic microstructure with a significant amount of second-phase particles between the laths and on the grain boundaries. These second-phase particles were speculated to be rich in carbon, resulting in the formation of martensite/austenite (MA) particles. The particles are visible in Figures 34 and 35 in the bright ferrite matrix. Bright and dark field micrographs (Figure 36A and B) illustrate a grain boundary which has a high density of coarse copper precipitates and some retained austenite. These coarse particles were predominantly located at the lath and grain boundaries.

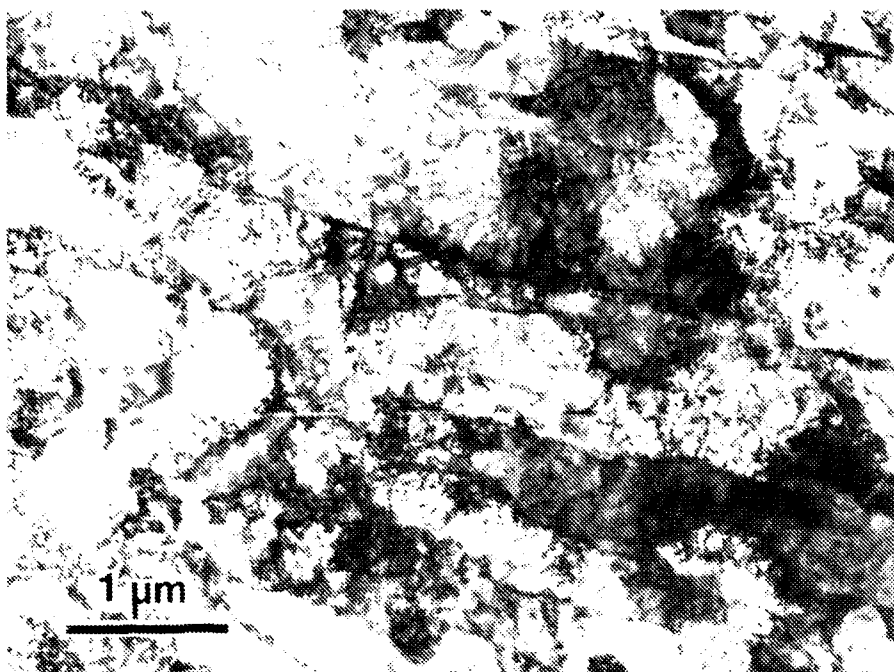


Figure 31. **TEM Micrograph Indicating Recovery in the Coarse HAZ After Stress Relieving**

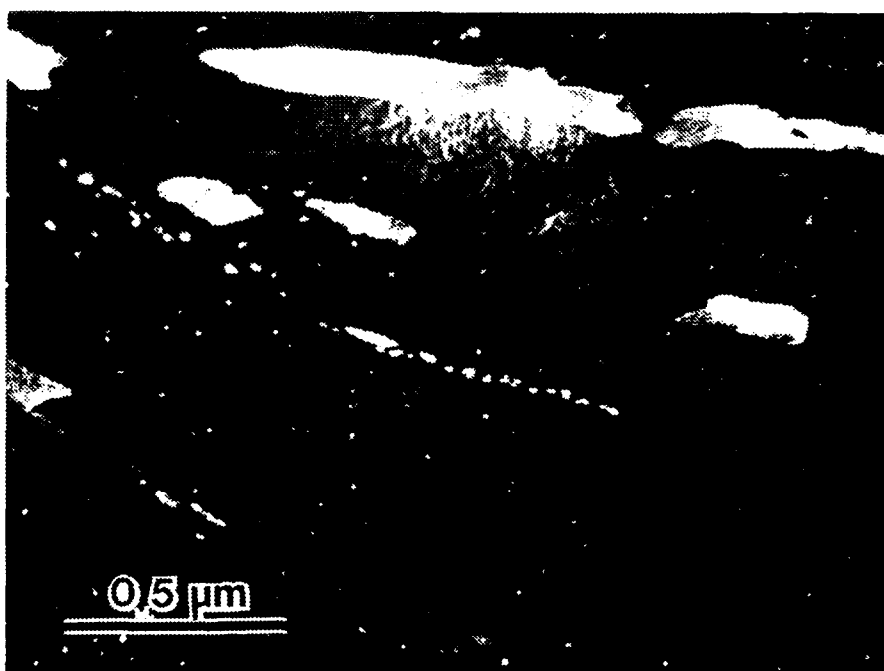
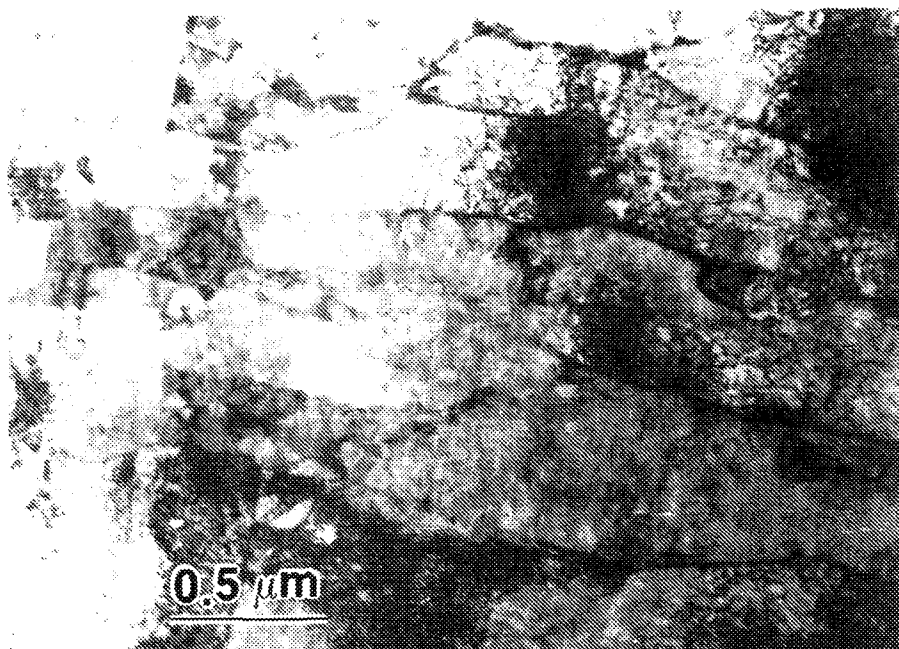


Figure 32. **TEM Micrograph Indicating Retained Austenite**



A



B

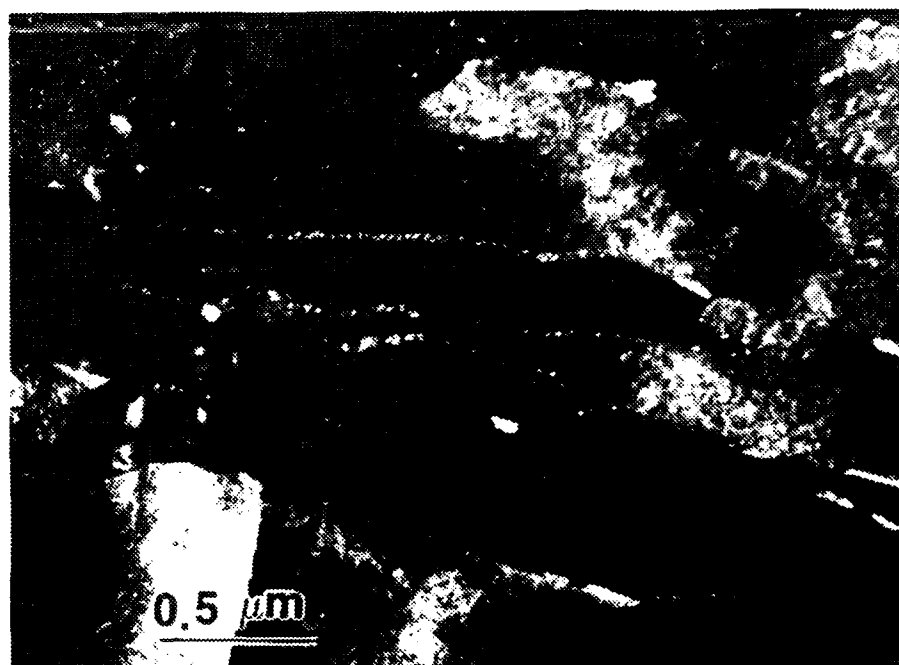
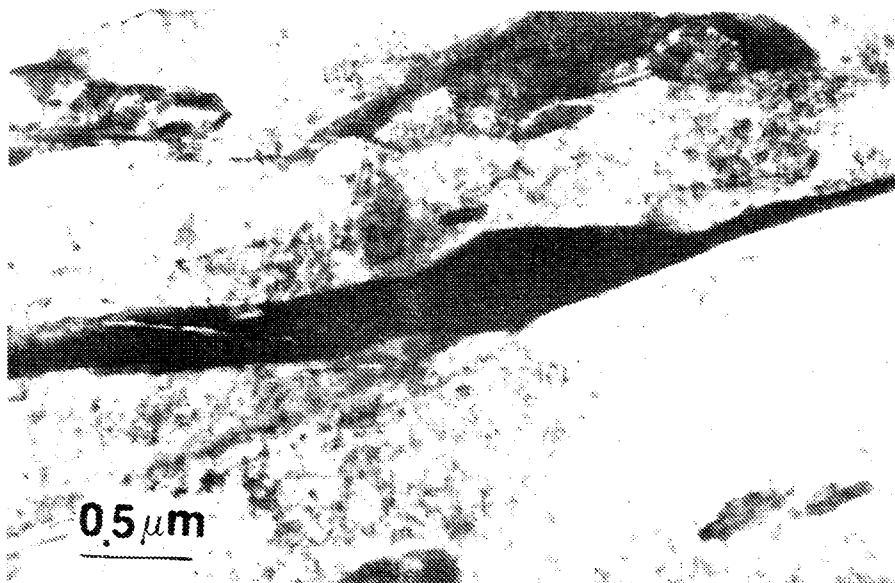
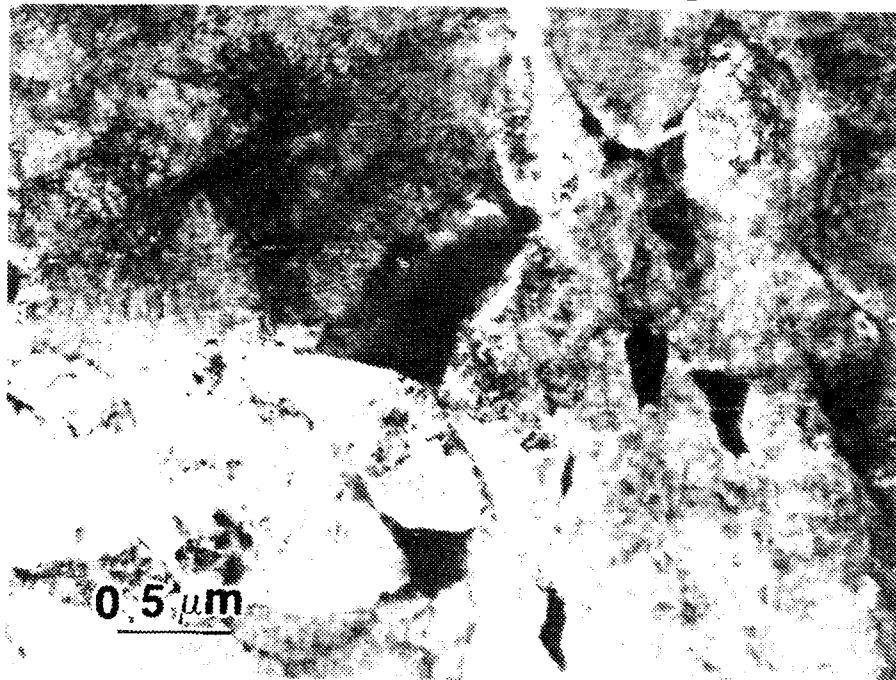


Figure 33. A **Bright Field Micrograph Showing the Lath Morphology**  
B **Dark Field Micrograph Illuminating the Copper Pre-  
cipitation on the Lath Boundary**



**Figure 34. TEM Micrograph of the Fusion Line Indicating a Lath Morphology and Relatively Large Second-Phase Particles (Dark Region)**



**Figure 35. TEM Micrograph of the Fusion Line Indicating a Disrupted Morphology with Second-Phase Particles on the Grain Boundary and Within the Grains**

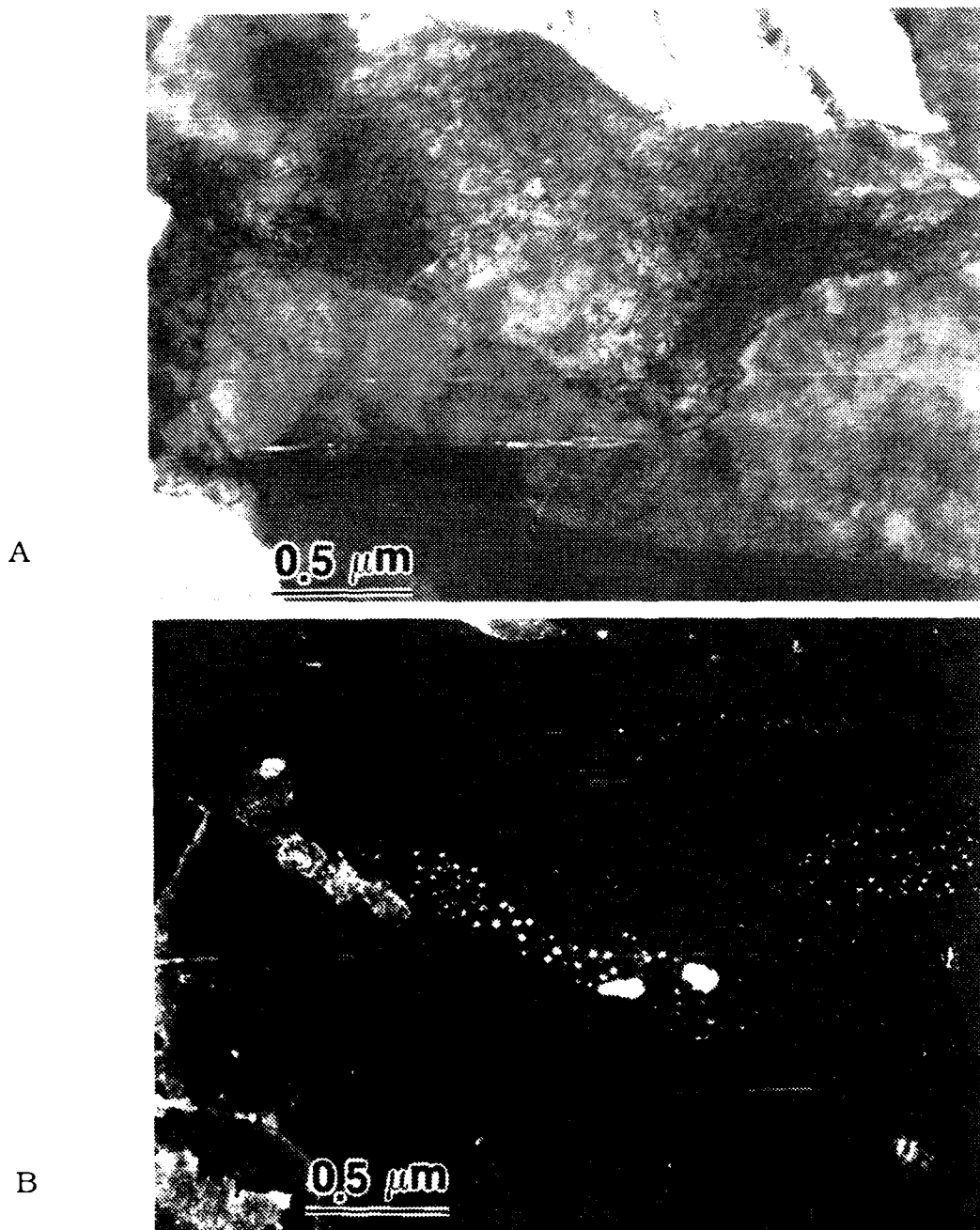


Figure 36. A **Bright Field Micrograph of a Grain Boundary Near the Fusion Line After Stress Relieving for One Hour at 650° C**

B (B) **Dark Field Micrograph of the Same Area Illuminating the Coarse Copper Precipitates and Retained Austenite on the Grain Boundary**

### **E. ROOM-TEMPERATURE TENSILE TESTING**

Two of the machined tensile specimens were tested on a Instron testing machine using a strain rate of  $8.5 \times 10^{-4}$  mm/(mm s). The stress vs. strain curves indicate tensile strengths of 794 and 799 MPa (Figure 37) which correlates well with the results obtained by DTNSRDC [Ref. 3]. The yield strength was 750 MPa and the fracture strength was 563 MPa for the two specimens. Both specimens failed in the base metal and exhibited similar necking and fracture appearance. Significant splitting occurred parallel to the rolling direction and perpendicular to the rolling plane (Figure 38). The gauge length showed uniform plastic deformation with the exception of the necked area and the weldment. This confirmed the integrity and higher strength level of the weld zone.

### **F. STRESS-RELIEF CRACKING**

The temperatures investigated were 550°, 600°, and 650° C. These temperatures were selected because they spanned the range of thermal relief quoted in the literature [Ref. 5].

The Materials Testing System (MTS) was initially utilized to conduct simple high temperature tensile testing of the specimens at 550° C and 650° C to determine the corresponding fracture strength at each temperature. The fracture strengths obtained were approximately 520 MPa at 550° C and 340 MPa at 650° C. These values were then used as a first approximation as the maximum stress levels for the initial loading of the test specimens during stress relief testing.

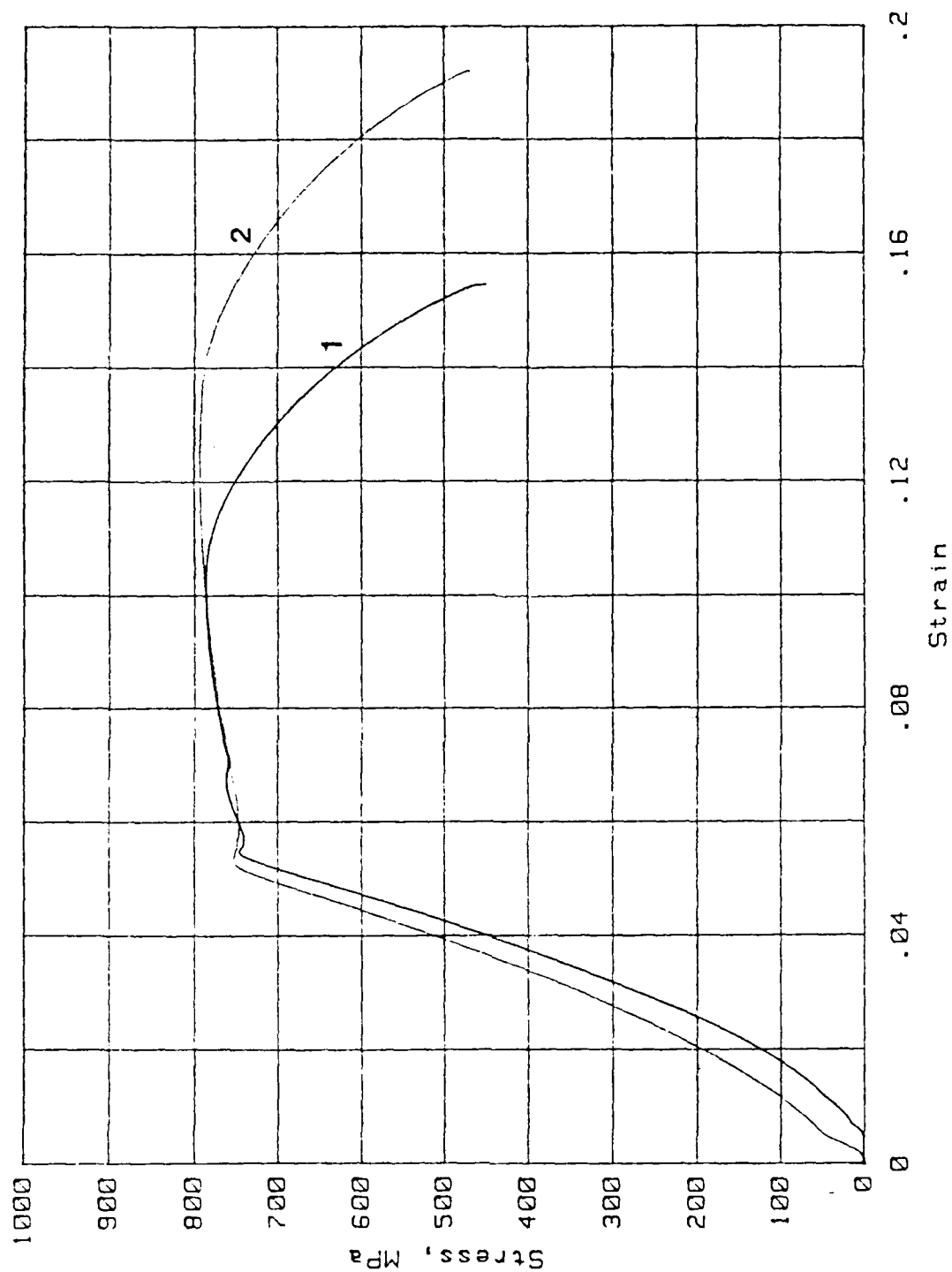


Figure 37. Room Temperature Stress Strain Curve  
for HSLA-100 Steel Weldments

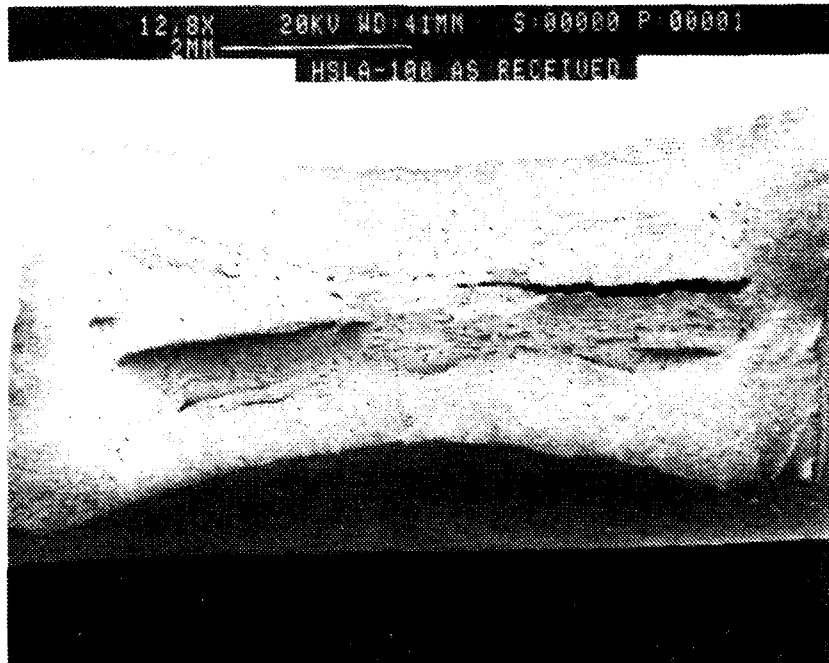


Figure 38. **SEM Low Magnification Fracture Surface of Flat Specimens, Fractured at Room Temperature in the Base Metal**

At a stress relief temperature of 650° C, some of the samples failed upon rapid heating at stress levels below 230 MPa. This stress level represented only 68 percent of the initially measured fracture strength.

The stress relief observed as a function of time is plotted, for the different test temperatures and initial stress levels, in Figures 39, 40, 41, and 42. The numerical data collected from the stress relief curves used for these plots is given in Table 3. A larger thermal relief rate was observed for the higher temperatures. The amount of stress relief was also observed to be a function of the applied stress because the decrease in the initial stress was higher for a larger initial load.

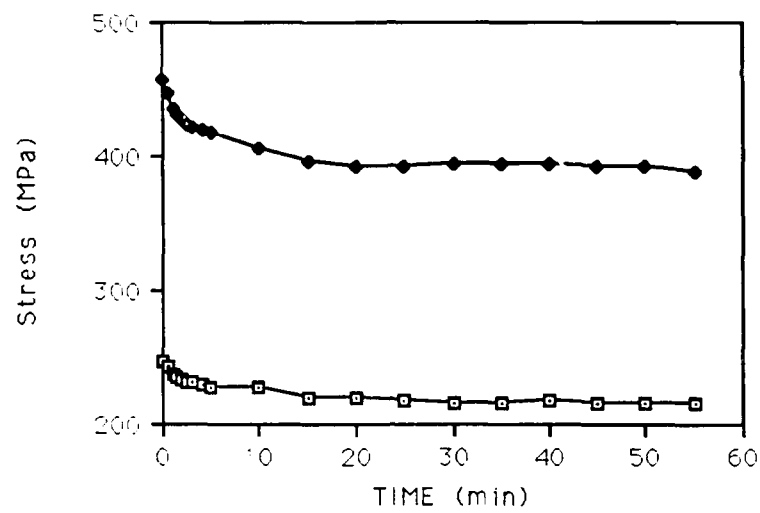


Figure 39. **Stress Relief Curves for Testing Conducted at 550° C**

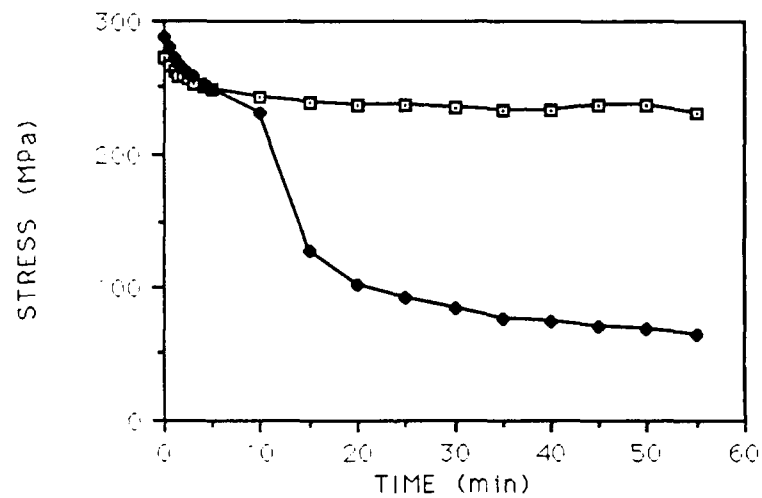


Figure 40. **Stress Relief Curves for Testing Conducted at 600° C**

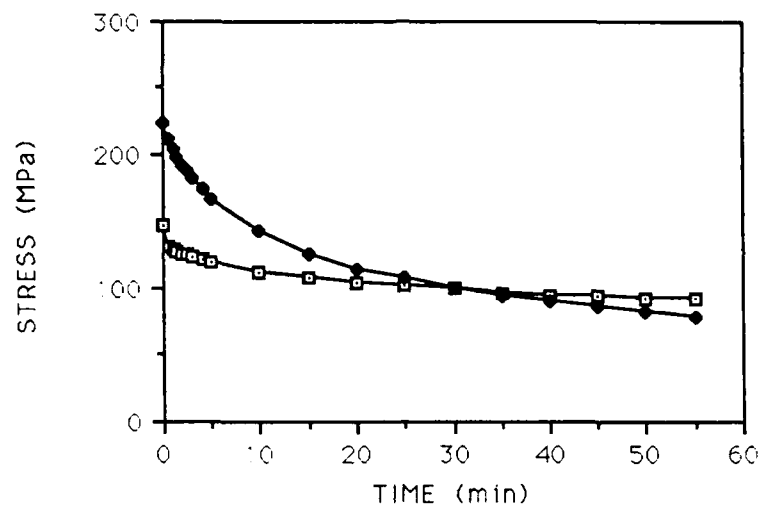


Figure 41. **Stress Relief Curves for Testing Conducted at 650° C**

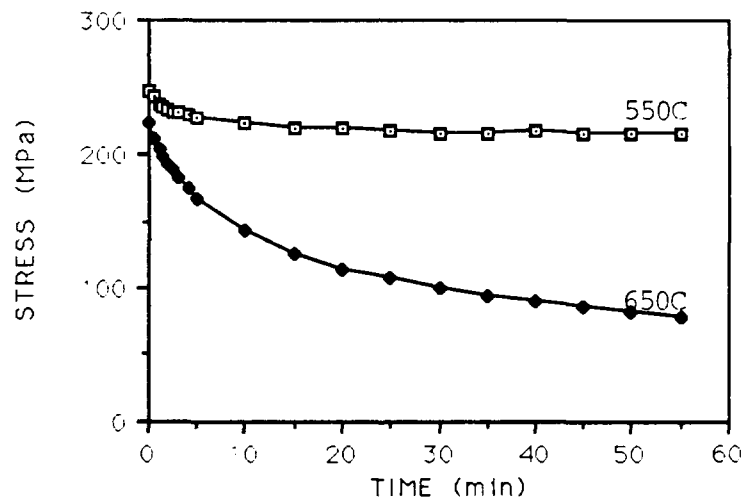


Figure 42. **Comparison of Stress Relief Curves for Two Different Test Temperatures**



TABLE 3

**STRESS RELIEF DATA AS A FUNCTION  
OF TIME AND TEMPERATURE**

Time (min.)	Stress (MPa)					
	550° C		600° C		650° C	
0.0*	248.0	457.5	273.0	287.7	146.1	222.7
0.5	242.5	446.5	265.7	281.1	132.3	211.7
1.0	237.0	435.4	262.4	272.3	129.0	203.9
1.5	235.4	430.5	259.1	267.9	126.8	198.4
2.0	233.7	426.6	258.0	265.1	125.7	192.9
2.5	231.5	424.4	265.0	261.3	124.6	187.4
3.0	230.4	422.2	253.6	259.1	123.5	183.0
4.0	229.3	418.9	250.2	253.6	121.0	174.2
5.0	228.2	416.7	249.1	248.4	119.1	167.6
10.0	227.7	405.7	242.5	230.4	112.4	142.2
15.0	220.5	396.9	239.2	127.9	107.5	125.7
20.0	218.8	391.4	237.0	102.5	104.2	114.6
25.0	217.2	392.5	238.1	91.5	101.4	106.9
30.0	216.6	394.7	235.4	84.9	99.2	100.3
35.0	216.1	394.7	233.7	77.2	97.0	93.9
40.0	216.9	393.6	233.6	75.0	94.8	90.4
45.0	215.5	391.4	237.0	71.1	93.2	86.0
50.0	215.3	391.4	237.0	68.3	92.1	82.7
55.0	215.0	389.1	231.5	64.5	91.5	78.3
60.0	214.8	385.8	234.8	61.2	88.2	75.5

\*The initial stress level used for stress relief testing.

A summary of the starting stress levels at each temperature is given in Table 4. The superscripts on the various stress levels denote the effect of the stress relief experiment on each specimen.

The observed crack profiles on the surface of the specimens tested were always intergranular and confined to the coarse grained HAZ, Figure 43. The cracks were generally observed to predominantly

TABLE 4

**INITIAL STRESS LEVELS AT EACH TEMPERATURE FOR  
STRESS RELIEF TESTING OF HSLA-100 WELDMENTS**

<b>Temperature (°C)</b>	<b>Stress Levels Investigated (MPa)</b>
550	255 <sup>a</sup> -469 <sup>c</sup>
600	255 <sup>a</sup> -290 <sup>b</sup> -331 <sup>c</sup>
650	186 <sup>b</sup> -193 <sup>c</sup> -221 <sup>d</sup> -228 <sup>c</sup> ->235 <sup>d</sup>

Explanation of Superscripts:

- a. No observed cracking
- b. Limited grain boundary separation
- c. Cracking visible to unaided eye
- d. Failed quickly after heat was applied

HAZ, Figure 43. The cracks were generally observed to predominantly run perpendicular to the applied stress (to be relieved). The cracks at a 550° C stress relief temperature were observed to branch (Figure 44), stop and start in distinct jumps (Figure 45), penetrate the weld metal (Figure 46), and be arrested by the weld metal (Figure 47). Although cracks were observed to penetrate the weld metal, this was not a predominant feature and when the crack did enter this region of the weldment it was not observed to travel a distance greater than 0.135 mm.

The fracture surfaces of the specimens subjected to the thermal relief experiment were found to contain a brittle region and a softer, more-ductile area. The coarse-grained HAZ, in the center of the



Figure 43. Crack Traversing the Coarse HAZ Perpendicular to the Load at a Test Temperature of 550° C

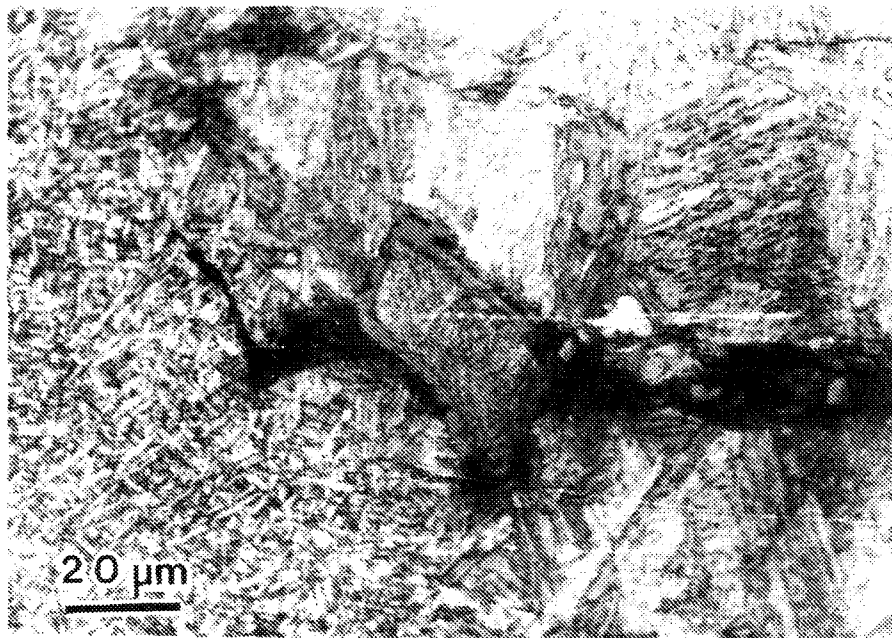


Figure 44. **Crack Branching After Stress Relieving at 550° C for One Hour**

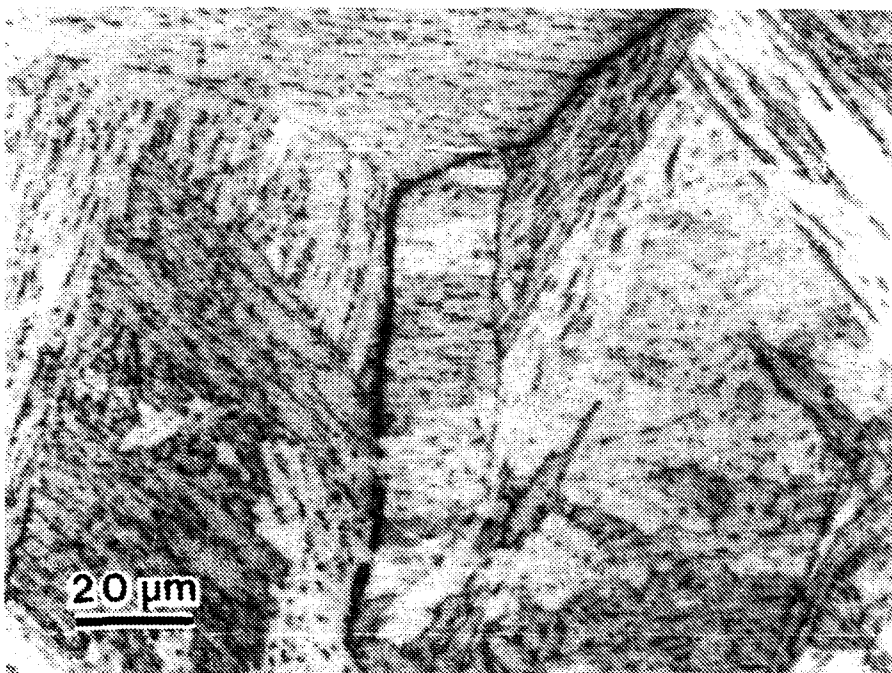


Figure 45. **Apparent Crack Discontinuities After Stress Relieving at 550° C**

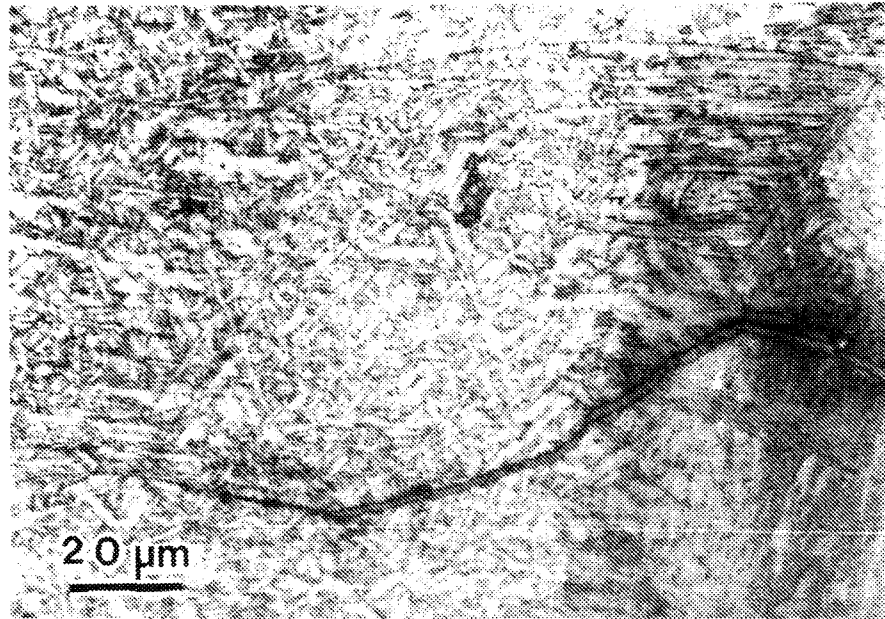


Figure 46. **Crack Penetration in the Weld Metal  
After Stress Relieving at 550° C**

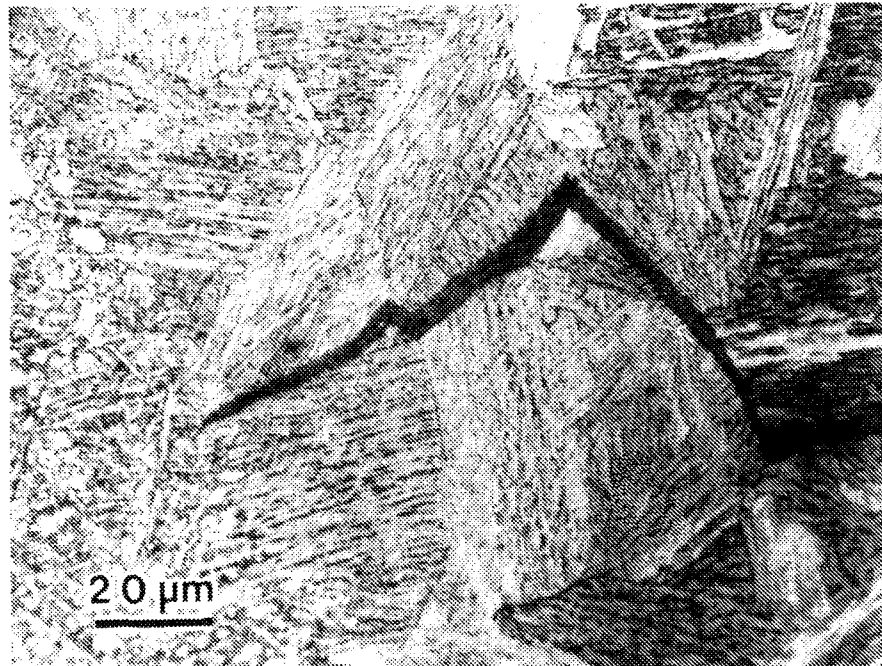


Figure 47. **Crack Arrested by the Weld Metal  
During Stress Relieving at 550° C**

weldment, was associated with the brittle region (Figures 48 and 49), whereas the ductile zone was evident on either side of this center area. SEM fractography exhibited the smooth, featureless grain boundary facets (Figures 50, 51, and 52) in the brittle region and dimples associated with ductile tearing in the region which plastically deformed (Figure 53).

#### **G. AUGER ELECTRON SPECTROSCOPY**

Two samples were sent to Naval Weapons Center, China Lake for Auger analysis of the fracture surface. The specimens were loaded to similar levels (221-228 MPa), but one failed upon heating (Specimen 1) to 650° C while under a fixed stress of 221 MPa, i.e., with no stress relief time. The other was stress relieved for one hour at 650° C then cooled and pulled to failure at ambient temperature (Specimen 2). Both fracture surfaces indicated a brittle intergranular region in the center of the weldment, but the sample which failed upon heating showed extensive plastic deformation in the weld metal.

The Auger analysis was primarily performed in the survey and profile modes. Specimen 1 indicated significant carbon, nickel, and copper concentrations on the fracture surface along with spherical Si particles. The depth of these concentrations in Specimen 1 was estimated to be less than 100 Å (Figure 54), while Specimen 2 showed a depth of 400 Å. Specimen 2 indicated the presence of S, Cl, N, O, Fe, and Cu (Figure 55). Copper was found everywhere on the fracture surface, with concentrations on the grain boundary facets and grain boundary edges.

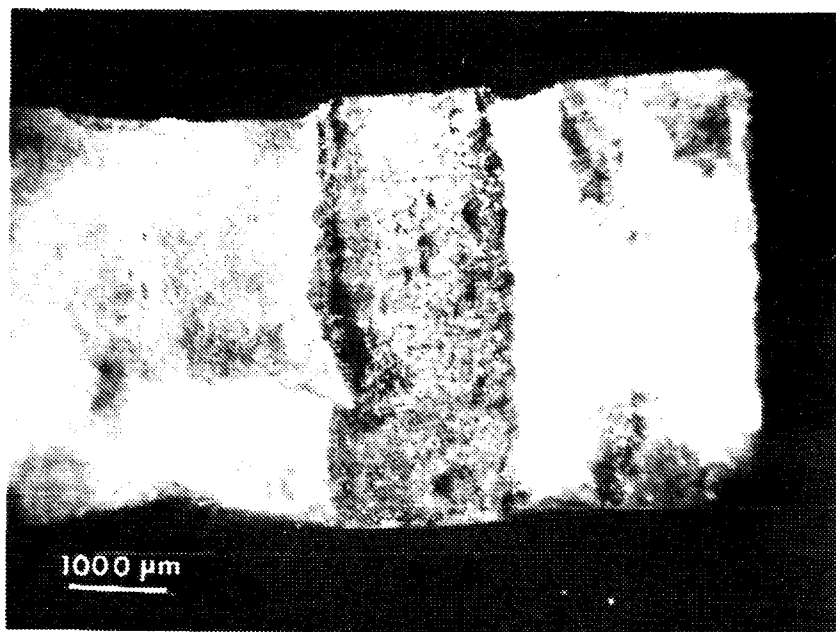


**Figure 48. Photograph of the Fracture Surface Illustrating Limited Lateral Plastic Flow in the Coarse-Grained HAZ**

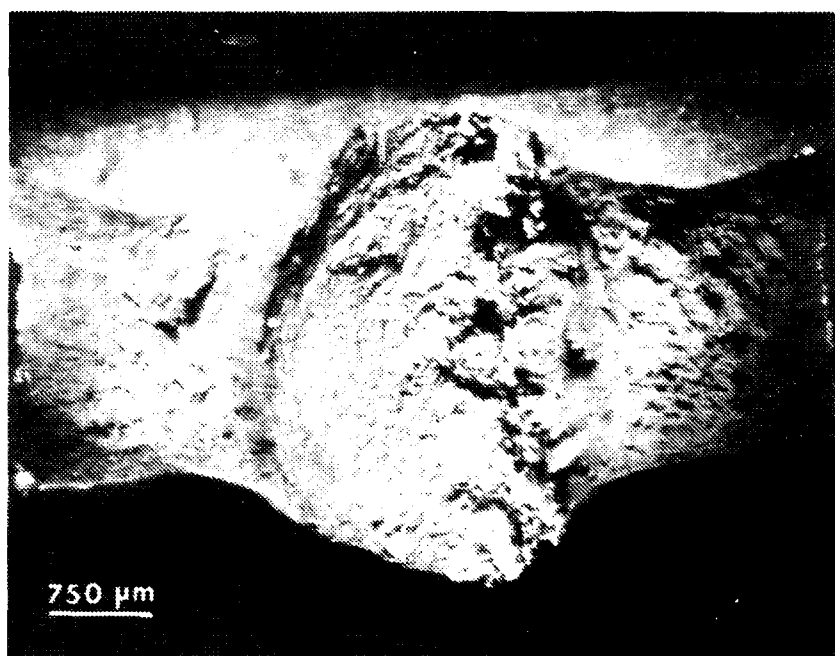


**Figure 49. Photograph of the Fracture Surface Illustrating More Plastic Flow in Areas Surrounding the Coarse-Grained HAZ**

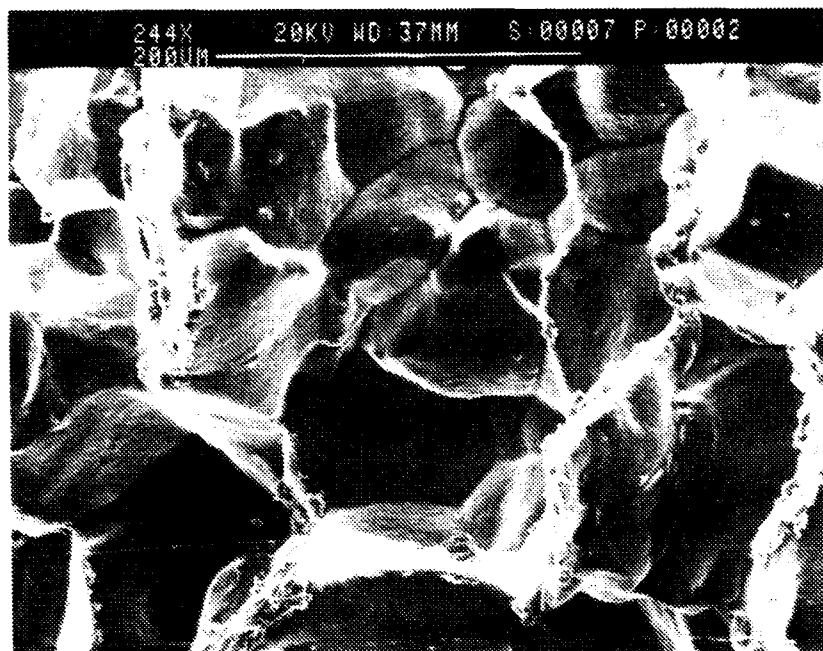


**Figure 50. SEM Micrograph Showing a Fracture Surface in the Coarse-Grained HAZ After Stress Relieving for One Hour at 550° C**

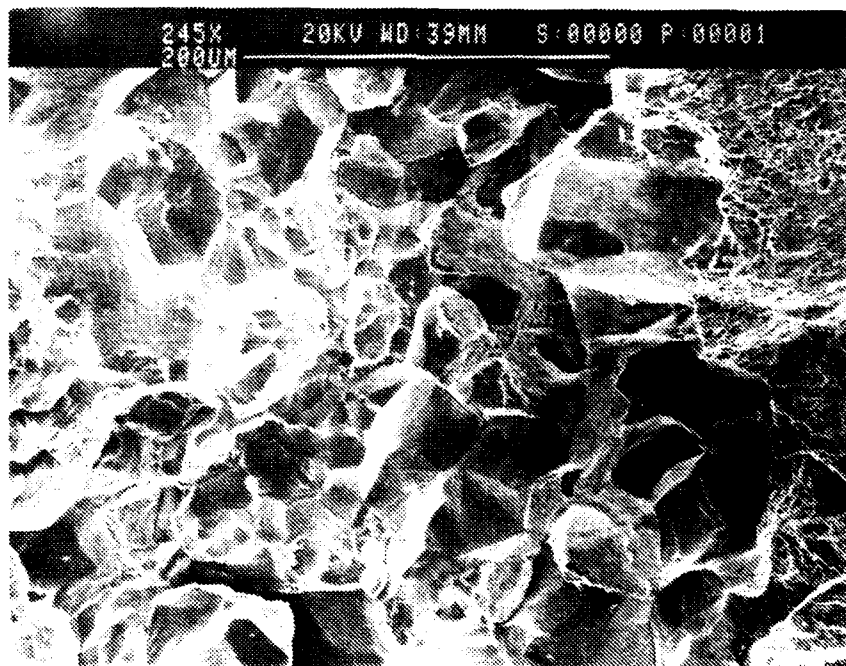


**Figure 51. SEM Micrograph of the Fracture Surface in the Coarse-Grained HAZ After Stress Relieving for One Hour at 600° C**



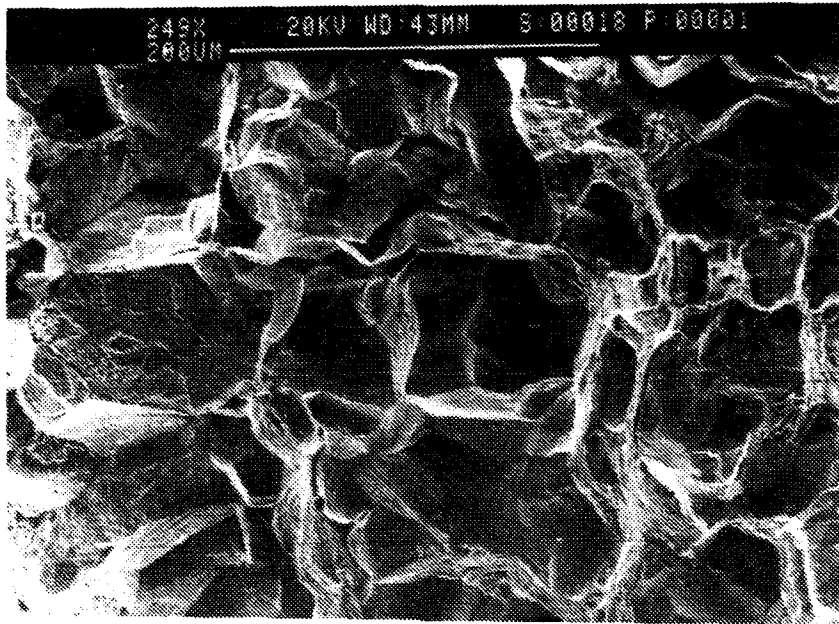


Figure 52. **SEM Micrograph of the Fracture Surface in the Coarse-Grained HAZ After Stress Relieving for One Hour at 650° C**

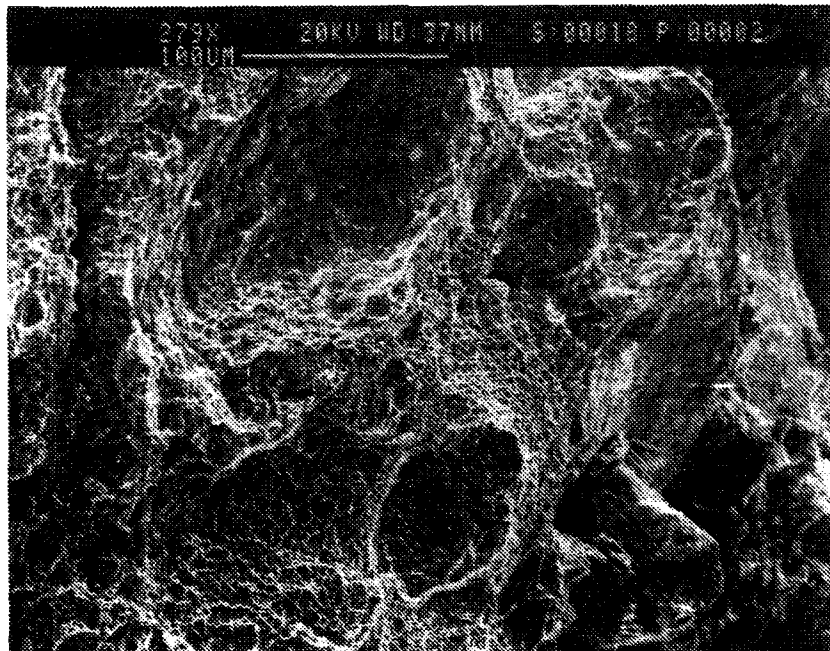


Figure 53. **SEM Micrograph Illustrating Ductile Fracture Typical of Certain Areas of the Fracture Surfaces At All Test Temperatures**

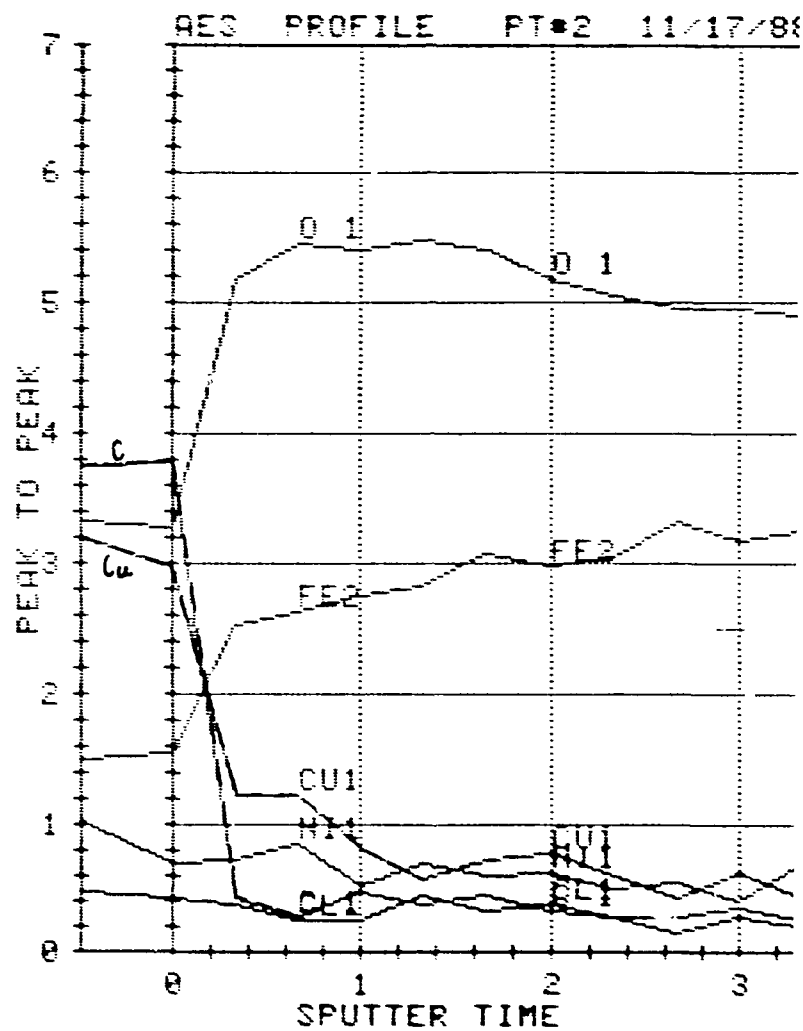


Figure 54. AES Depth Profile on the Grain Boundary Face of Specimen 1

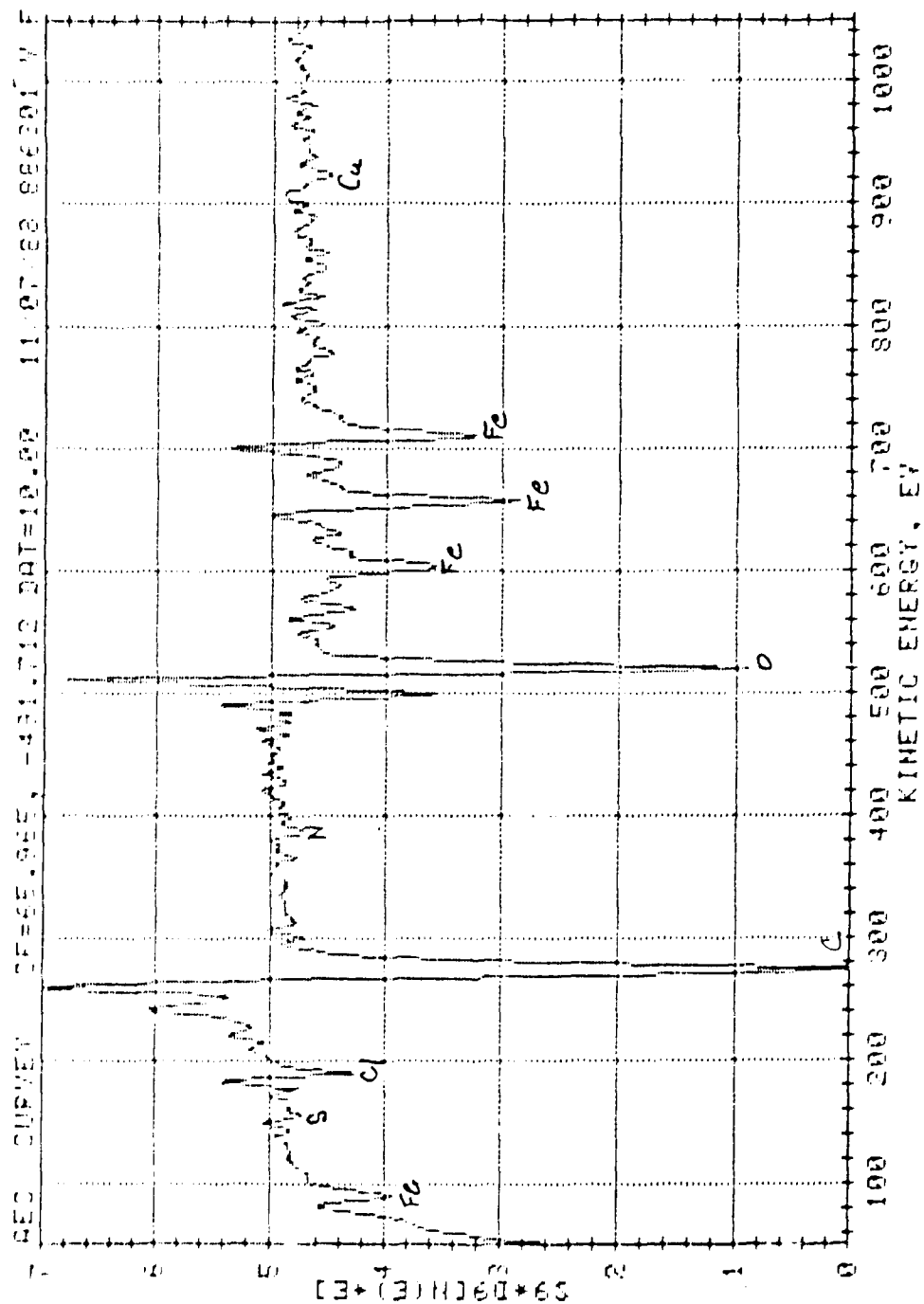


Figure 55. AES Survey Showing the Elements Present  
 on the Fracture Surface of Specimen 2

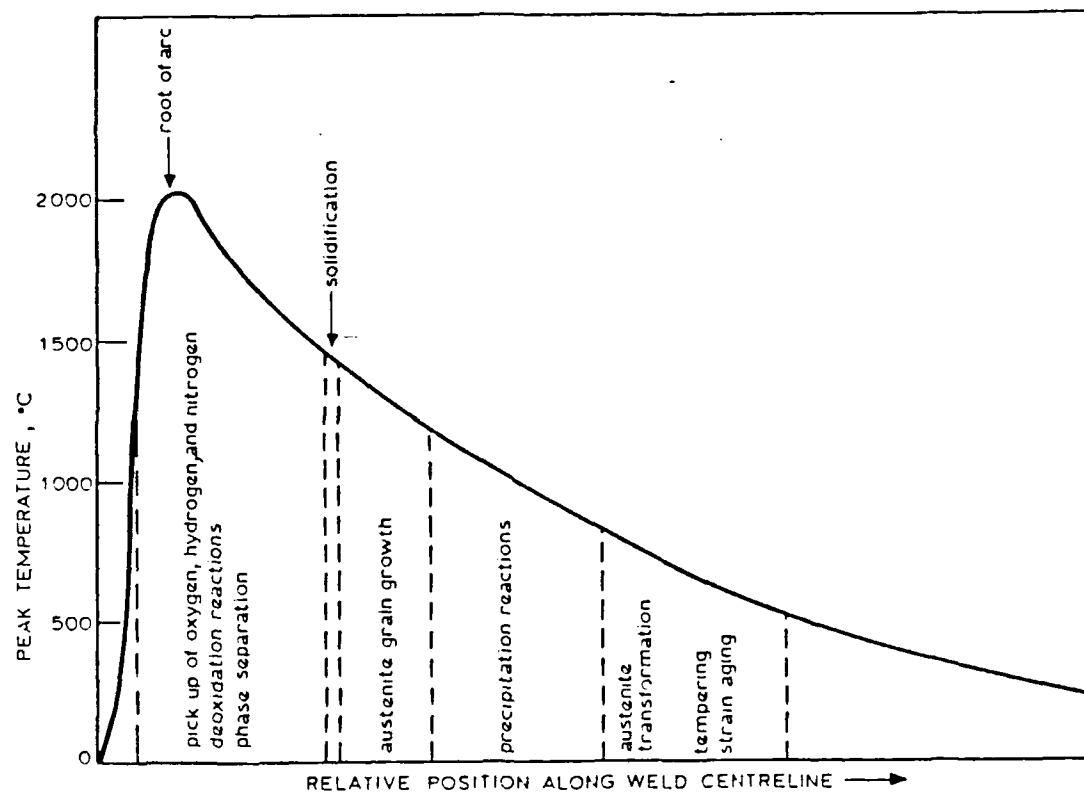
## **V. DISCUSSION**

The microstructure of the heat-affected zone of HSLA-100 steel will be discussed and related to its mechanical properties. This will then be used to discuss the microhardness profiles and the observed stress-relief cracking.

### **A. MICROSTRUCTURE**

The microstructure formed in the HAZ is a consequence of the composition of the steel and the thermal cycle or cycles resulting from welding. Austenite grain growth occurs in the base metal which is close to the weld bead (Figure 56). A driving force for a strain-free material is accomplished by austenite grain growth which is accompanied by a reduction in surface energy. Growth may, however, be inhibited by the presence of niobium-carbides which are stable at high temperature. The bainite grows as packets, in the large austenite grains, of almost parallel, low-angle laths (Figures 19, 20, 21). This microstructure has a high dislocation density which imparts high strength. [Refs. 35, 36]

The HAZ grain size, strength, and toughness will depend on the overlap of adjacent weld passes. It is possible to re-normalize the hard, coarse-grained bainite by multipass welding which subjects the HAZ to lower temperature thermal cycles. The HAZ becomes a combination of quenched and tempered zones containing coarse grains, fine grains.



Characteristic temperature ranges where specific chemical and physical reactions occur during cooling of weld metal down to room temperature are also indicated.

**Figure 56. Schematic Diagram Illustrating Weld Centerline Peak Temperature at Different Distances From Root of Arc [Ref. 35]**

and a recovered structure. This situation reduces the residual strain, thereby increasing the toughness. [Refs. 26, 36]

## **B. MICROHARDNESS PROFILES**

In the as-received condition, the hardness of the weld metal is attributed to the acicular ferrite morphology, which derives its strength and toughness from the fine interlocking ferrite plates, and a high dislocation density. The high hardness of the coarse HAZ is a result of the fine copper precipitation (Figure 22) and the high dislocation density in the bainitic matrix. The increased hardness of the coarse HAZ in traverse BB (Figure 13) can be attributed to an essentially quenched microstructure. The decreasing hardness from the fusion line towards the unaffected base metal can be correlated to the thermal cycling experienced from the 12 weld passes. The fine-grained HAZ never exceeds the  $A_{c1}$  temperature (Figure 56), so the  $\alpha$  to  $\gamma$  transformation will not occur. Thermal cycling in this region results in particle growth and dislocation annihilation, which account for the decreasing hardness.

A decrease in microhardness measurements obtained from the center of the weldment after stress relieving for one hour at 650° C has been observed in the fine-grained HAZ region and base metal. This can be attributed to further aging and recovery taking place. The excellent resistance of this alloy to tempering is illustrated in this area by the very slight decrease in hardness upon stress relief testing.

The weld metal was extensively tempered by the subsequent weld passes. However, the hardness in this area does not exhibit any effect

from the further tempering associated with the stress-relief temperature.

The heat-affected zone has a higher hardness throughout the entire coarse-grained region after stress-relief testing. It is difficult to explain this trend because copper had already precipitated out of solution during the thermal cycles experienced during welding. This can be confirmed by the TEM micrographs of this area (Figure 22), which illustrate uniform precipitation throughout this area prior to stress-relief testing. Goodman, et al. have demonstrated that when the copper particles are visible through the TEM, the alloy is in the over-aged condition [Refs. 21, 22]. If this is true, no further increment in hardening is expected. In addition, the region may have experienced some further rearrangement and annihilation of the dislocations, making the area even softer.

The microhardness profiles all indicate a weld metal hardness, hence strength, greater than the base metal. This is in good agreement with the room-temperature tensile fractures which were all located in the base metal. This was observed for the specimens pulled before and after stress-relief testing. The high hardness in the coarse-grained HAZ can be translated into improved load-carrying ability. It has also been postulated that the segregation of impurities to the grain boundary at high temperature is not sufficient to promote intergranular fracture because the final fracture occurs in the base metal [Ref. 29].

### C. STRESS-RELIEF CRACKING

Stress-relief treatments are often used after welding to reduce residual stresses. At the high temperatures experienced in welding, the copper precipitates next to the fusion line go into solution in the growing austenite grains (Figure 56). During cooling to ambient temperatures, the precipitates remain in solution. The strength of HSLA-100 can increase considerably during the thermal cycling associated with multipass weldments. This results from the subsequent precipitation of the coherent clusters of copper in the bcc ferrite matrix. [Refs. 19, 21, 22]

The matrix strengthening from the copper precipitation transfers the creep strain to the prior austenite grain boundary at the thermal relief temperature. Intergranular precipitates which rapidly form, as observed in Figures 33 and 36, restrict grain boundary sliding in the coarse-grained HAZ so that intergranular voids form. This results in a loss of creep ductility, which is significantly reduced by the segregation of impurity elements such as phosphorous to the grain boundaries [Ref. 5]. Stress-relief cracking occurs when the creep ductility is insufficient to accommodate the strains developed by the pinning of these grain boundaries. [Refs. 4, 5, 30]

The mechanism discussed above has been used to describe post-weld heat-treatment cracking in low-alloy (2.25 Cr-Mo-V, Mn-Mo-Ni) and copper-precipitation strengthened HSLA steels [Refs. 4, 5, 29, 30, 36, 37]. The cracking has always been reported in the coarse-grained region of the HAZ and has a tendency to initiate at geometrical



discontinuities such as the center of a double V joint [Ref. 37]. These two factors were both satisfied in the observed cracking of HSLA-100. The stress-relief cracking was most pronounced in the center of the double 60° bevel.

Recent studies suggest that the Low Ductility Intergranular Fracture (LDIGF) mode is promoted by increasing concentrations of impurity elements at the grain boundaries [Ref. 5]. Auger Electron Spectroscopy (Figures 54 and 55) confirms the presence of high quantities of alloying elements on the boundaries of these fracture surfaces. The LDIGF mode of fracture was observed in the coarse HAZ at all three temperatures (Figures 50, 51, and 52). The Intergranular Micro Void Coalescence (IGMVC) mode was not observed on any of the fracture surfaces. This is consistent with the literature as IGMVC occurs at temperatures above 600° C and only in very small regions. [Ref. 29]

The average austenite grain size in the coarse-grained HAZ was measured to be 54 microns, which is typical of a susceptible HAZ grain size [Ref. 29]. The observed cracking in this investigation was essentially confined to the island of coarse grains located in the center of the weldment, which exhibited a well-defined grain boundary upon etching. This phenomenon has also been reported in the literature and has been attributed to a lower susceptible microstructure to stress-relief cracking due to the thermal cycling associated with multipass welds. [Ref. 29]

The inconsistencies of the specimens failing upon heating to the test temperature of 650° C could not be resolved with the limited number of tensile specimens. However, an explanation for the fracture which occurred upon heating is the formation of austenite at the boundaries during the thermal cycling of the weldment. The segregation of alloying elements, such as nickel, copper, and carbon, to the grain boundary, as confirmed by Auger spectroscopy, influences the austenite formation temperature. TEM analysis, however, indicated the presence of retained austenite on the boundaries both before and after stress-relief testing was conducted. The nickel and to a lesser extent the copper are austenite formers. The high concentration of these elements will cause the stability of austenite at a lower temperature. An empirical equation has been developed for the determination of the eutectoid temperature based on the composition of the steel and is given as Equation 2 [Ref 38].

$$Ac_1 = 723 - 10.7 \text{ Mn} - 16.9 \text{ Ni} - 29.1 \text{ Si} - 16.9 \text{ Cr} \dots \quad (2)$$

where:  $Ac_1$  in degrees C

Elements are in weight %

The  $Ac_1$  temperature for HSLA-100 has been calculated to be 671° C. The high concentrations of nickel on the austenite grain boundaries (where austenite was observed) could conceivably lower the  $Ac_1$  temperature below the test temperature of 650° C. If this occurred, then the failures upon heating to stress-relieving temperatures may be attributable to an overloading of the weaker austenite.

A possible explanation of why this type of failure does not occur at room temperature is that the austenite may transform to other microconstituents on cooling or it may transform to martensite upon deformation during the tensile test.

## VI. CONCLUSIONS

1. HSLA-100 steel is susceptible to Stress Relief Cracking (SRC) at all three temperatures studied (i.e., 550°, 600°, and 650° C).
2. In all instances, the cracks were observed to be intergranular in nature.
3. The coarse-grained heat-affected zone appears to be more susceptible to intergranular fracture than the fine-grained HAZ. This may be attributed to the smaller grain boundary area in the coarse HAZ.
4. A high concentration of alloying elements (C, Cu, Ni) was observed on the grain boundaries. The thickness of this alloy-enriched layer increased after stress-relief testing.
5. Cracking was only observed to occur in a narrow band of stresses at all three temperatures investigated.

## LIST OF REFERENCES

1. Anderson, T. L., Hyatt, J. P., and West, J. C., "The Benefits of New High-Strength Low-Alloy (HSLA) Steels," *Welding Journal*, pp. 21-26, September 1987.
2. Kvidahl, L. G. "An Improved High Yield Strength Steel for Shipbuilding," *Welding Journal*, v. 64, pp. 42-48, July 1985.
3. David Taylor Research Center, Report TM-28-88/03, *Certification of HSLA-100 Steel for Structural Applications*, by E. Czyryca, R. Link, and R. Wong, pp. 1-104, January 1988.
4. Lundin, C. D., Menon, R., and Chen, Z., *Postweld Heatreatment Cracking in A710 HSLA Precipitation Strengthened Steel*, paper presented at the 1986 Gatlinburg Conference International Trends in Welding Research, Gatlinburg, Tennessee, 1986.
5. Edwards, R. H., Barbaro, F. J., and Gunn, K. W., "Stress Relief in Cr-Mo-V Steels," *Metals Forum*, v. 5, no. 2, pp. 119-129, 1982.
6. Krishnadev, M. R., "Development and Characterization of a New Family of Copper-Containing HSLA Steels," *HSLA Steels Technology & Applications*, American Society for Metals, pp. 132-133, 1983.
7. AMAX Materials Research Center, Report CPR-20, *Development of 100 KSI Yield Strength HSLA Steel*, by A. P. Colden and T. B. Cox, pp. 2-13, July 1986.
8. David Taylor Research Center, Report SME-87/83, *Trial Production of HSLA-100 Steel*, E. J. Czyryca, pp. 2-22, February 1988.
9. AMAX Materials Research Center, Report C0021, *Phase II Report and Phase III Commercial Plate Documentation*, A. P. Colden and T. B. Cox, pp. 1-5, June 1987.
10. Leslie, W. C., *The Physical Metallurgy of Steels*, McGraw-Hill International Book Company, pp. 189-210, 1982.
11. Lemay, I., and Krishnadev, M. D., *Copper in Iron and Steel*, Wiley-Interscience, pp. 5-43, 83-133, 1982.

12. Pickering, F. B., *Physical Metallurgy and the Design of Steels*, Applied Science Publishers Ltd., pp. 60-87, 1978.
13. Lemay, I., Schetky, L., and Krishnadev, M. R., "The Role of Copper in HSLA Steels: A Review and Update," *High Strength Low Alloy Steels*, pp. 64-67, August 1984.
14. Wilson, A. D., and Taylor, W. G., "A710: A High Strength, Low Carbon Alloy Steel for Offshore Applications," *OTC '85 Proceedings*, 1985 Offshore Technology Conference, Houston, Texas, May 1985.
15. Jesseman, R. J., and Murphy, G. J., "Mechanical Properties and Precipitation Hardening Response in ASTM A710 Grade A and A736 Alloy Steel Plates," *HSLA Steel Technology & Applications*, American Society for Metals, pp. 655-665, 1983.
16. Miglin, M. T., Hirth, J. P., Rosenfield, A. R., and Clark, W. A., "Microstructure of a Quenched and Tempered Cu-Bearing High Strength Low-Alloy Steel," *Metallurgical Transactions*, v. 17A, pp. 791-798, May 1986.
17. Hornbogen, E., "Role of Strain Energy during Precipitation of Copper and Gold from Alpha Iron," *Metallurgica*, v. 10, pp. 525-533, May 1962.
18. Hornbogen, E., and Glenn, R. C., "A Metallurgical Study of Precipitation of Copper from Alpha Iron," *Transactions of the Metallurgical Society of AIME*, v. 218, pp. 1064-1070, December 1960.
19. Hornbogen, E., "Aging and Plastic Deformation of an Fe-0.9% Cu Alloy," *Transactions of the ASM*, v. 57, pp. 120-132, 1964.
20. Speich, G. R., and Oriani, R. A., "The Rate of Coarsening of Copper Precipitate in Alpha-Iron Matrix," *Transactions of the Metallurgical Society of AIME*, v. 233, pp. 623-631, April 1965.
21. Goodman, S. R., Brenner, S. S., and Low, J. R., "An FIM-Atom Probe Study of the Precipitation of Copper from Iron-1.4 At. Pct. Copper. Part I: Field Ion Microscopy," *Metallurgical Transactions*, v. 4, pp. 2363-2370, October 1973.
22. Goodman, S. R., Brenner, S. S., and Low, J. R., "An FIM-Atom Probe Study of the Precipitation of Copper from Iron-1.4 At. Pct. Copper. Part II: Atom Probe Analysis," *Metallurgical Transactions*, v. 4, pp. 2371-2378, October 1973.

23. Hicho, G. E., Singal, S., Smith, L. C., and Fields, R. J., "Effect of Thermal Processing Variations on the Mechanical Properties and Microstructure of a Precipitation Hardened HSLA Steel," *HSLA Steels Technology & Applications*, American Society for Metals, pp. 705-713, 1983.
24. Easterling, K., *Introduction to the Physical Metallurgy of Welding*, pp. 156-219, Butterworth, 1983.
25. Myers, J., and Clark, J. N., "Influence of Welding Procedures on Stress Relief Cracking in Cr-Mo-V Steels: Part I Use of Cross Weld Specimens," *Metals Technology*, pp. 382-394, October 1981.
26. Stout, R. D., "Postweld Heat Treatment of Pressure Vessels," *Welding Research Council Bulletin*, no. 302, pp. 1-14, February 1985.
27. Van Vlack L. A., *Textbook of Materials Technology*, pp. 61, Addison Wesley Publishing Company, 1973.
28. Clark, J. N., and Myers, J., "Stress Relief Cracking in High Strength Structural Steel BS4360 Grade 55F," *Materials Science and Technology*, v. 4, pp. 610-612, July 1988.
29. You, C. P., Hipplesley, C. A., and Knott, J. F., "Stress Relief Cracking Phenomena in High Strength Structural Steel," *Metal Science*, v. 18, pp. 387-394, August 1984.
30. Swift, R. A., "The Mechanism of Stress Relief Cracking in 2.25 Cr-1Mo Steel," *Welding Research Supplement to the Welding Journal*, pp. 195s-200s, May 1971.
31. Meitzner, C. F., and Pense, A. W., "Stress Relief Cracking in Low Alloy Steel Weldments," *Welding Research Supplement to the Welding Journal*, pp. 431s-440s, October 1969.
32. Atlss Center, Lehigh University, Report No. 4, *Heat Affected Zone and Weldment Studies on A710 Steel*, January 1988.
33. Dhooge, A., and Vinckier, A., "Reheat Cracking—A Review of Recent Studies," *Int. J. Pres. Ves. & Piping*, no. 27, pp. 239-269, 1987.
34. Metals Handbook, Ninth Edition, v. 4, pp. 29,92, American Society for Metals, 1978.

35. Grong, O., and Matlock, D. K., "Microstructural Development in Mild and Low-Alloy Steel Weld Metals," *International Metals Reviews*, v. 31, pp. 27-46, 1986.
36. Alberry, P. J., Chew, B., and Jones, W. K. C., "Prior Austenite Grain Growth in Heat Affected Zone of a 0.5 Cr-Mo-V Steel," *Metals Technology*, pp. 317-325, June 1977.
37. Pense, A. W., Galda, E. J., and Powell, G. T., "Stress Relief Cracking in Pressure Vessel Steels," *Welding Research Supplement*, pp. 274s-378s, August 1971.
38. Andrews, K. W., "Empirical Formulae for the Calculation of Some Transformation Temperatures," *Journal of the Iron and Steel Institute*, pp. 721-727, July 1965.



# INITIAL DISTRIBUTION LIST

	<u>No. Copies</u>
1. Defense Technical Information Center Cameron Station Alexandria, VA 22304-6145	2
2. Library, Code 0142 Naval Postgraduate School Monterey, CA 93943-5002	2
3. Department Chairman, Code 69Hy Department of Mechanical Engineering Naval Postgraduate School Monterey, CA 93943-5000	1
4. Dr. Saeed Saboury P. O. Box 51922 Pacific Grove, CA 93950	2
5. Dr. J. M. B. Losz, Code 69Lo Department of Mechanical Engineering Naval Postgraduate School Monterey, CA 93943-5000	2
6. Professor T. R. McNelley, Code 69Mc Department of Mechanical Engineering Naval Postgraduate School Monterey, CA 93943-5000	1
7. Mr. Paul W. Holsberg, Code 2815 David Taylor Naval Ship Research and Development Center Annapolis, MD 21402-5067	1
8. Mr. E. J. Czyryca, Code 2814 David Taylor Naval Ship Research and Development Center Annapolis, MD 21402-5067	1

- |     |  |   |
|-----|--|---|
| 9.  | Capt. S. McNutt, CF<br>13 Paula Crescent<br>Nepean, Ontario, Canada K2H 8Y8  | 3 |
| 10. | Low Level Air Defence Project<br>National Defence Headquarters<br>Major-General George R. Pearks Building<br>Ottawa, Ontario, Canada K1A 0K2                     | 1 |
| 11. | Director Personnel Education and Development<br>National Defence Headquarters<br>Major-General George R. Pearks Building<br>Ottawa, Ontario, Canada K1A 0K2      | 1 |
| 12. | Director General Land Engineering and Maintenance<br>National Defence Headquarters<br>Major-General George R. Pearks Building<br>Ottawa, Ontario, Canada K1A 0K2 | 1 |
| 13. | Lt. M. H. Heinze, USN, Code N64<br>Commander Naval Surface Force, U.S. Pacific Fleet<br>NAB Coronado<br>San Diego, CA 92155-5035                                 | 1 |
| 14. | Capt. R. Perron, CF<br>71 Via Paraiso<br>Monterey, CA 93940  | 1 |